

# Consistent and Asymptotically Statistically-Efficient Solution to Camera Motion Estimation

Guangyang Zeng, Qingcheng Zeng, Xinghan Li, Biqiang Mu, Jiming Chen, Ling Shi, and Junfeng Wu

arXiv:2403.01174v1 [cs.CV] 2 Mar 2024

**Abstract**—Given 2D point correspondences between an image pair, inferring the camera motion is a fundamental issue in the computer vision community. The existing works generally set out from the epipolar constraint and estimate the essential matrix, which is not optimal in the maximum likelihood (ML) sense. In this paper, we dive into the original measurement model with respect to the rotation matrix and normalized translation vector and formulate the ML problem. We then propose a two-step algorithm to solve it: In the first step, we estimate the variance of measurement noises and devise a consistent estimator based on bias elimination; In the second step, we execute a one-step Gauss-Newton iteration on manifold to refine the consistent estimate. We prove that the proposed estimate owns the same asymptotic statistical properties as the ML estimate: The first is consistency, i.e., the estimate converges to the ground truth as the point number increases; The second is asymptotic efficiency, i.e., the mean squared error of the estimate converges to the theoretical lower bound — Cramer-Rao bound. In addition, we show that our algorithm has linear time complexity. These appealing characteristics endow our estimator with a great advantage in the case of dense point correspondences. Experiments on both synthetic data and real images demonstrate that when the point number reaches the order of hundreds, our estimator outperforms the state-of-the-art ones in terms of estimation accuracy and CPU time.

**Index Terms**—Camera motion estimation; essential matrix; epipolar geometry; maximum likelihood estimation; nonconvex optimization

## 1 INTRODUCTION

CAMERA motion estimation (CME) involves estimating the relative camera pose from two images. It serves as a building block in many visual odometry, structure-from-motion (SfM), and simultaneous localization and mapping (SLAM) systems [1]–[4]. A CME pipeline generally includes two modules [5]–[10]: The front-end extracts feature points

*G. Zeng, Q. Zeng, and J. Wu are with the School of Data Science, Chinese University of Hong Kong, Shenzhen, Shenzhen 518172, P. R. China. {zengguangyang, zengqingcheng, junfengwu}@cuhk.edu.cn.*

*X. Li and J. Chen are with the College of Control Science and Engineering and the State Key Laboratory of Industrial Control Technology, Zhejiang University, Hangzhou 310027, P. R. China. xinghanli0207@gmail.com, cjm@zju.edu.cn.*

*B. Mu is with Key Laboratory of Systems and Control, Institute of Systems Science, Academy of Mathematics and Systems Science, Chinese Academy of Sciences, Beijing 100190, China. bqmu@amss.ac.cn.*

*L. Shi is with the Department of Electronic and Computer Engineering, Hong Kong University of Science and Technology, Hong Kong. eesling@ust.hk.*

from input images and then conducts feature matching to produce 2D point correspondences; The back-end recovers the relative pose based on these point correspondences. In this paper, we focus on the back-end algorithm by assuming the point correspondences are given.

The existing literature generally estimates the essential matrix  $\mathbf{E}$  first, see (2), based on which the relative pose (including rotation matrix  $\mathbf{R}$  and translation  $\mathbf{t}$ ) is recovered. Due to the scale ambiguity caused by the unknown depths of measured points, the rotation matrix and the direction of translation can be recovered from the essential matrix, while the translation distance cannot be identified [1]. To further estimate the translation distance, a priori information about the 3D points should be provided, e.g., via a calibration board or constructed 3D structures.

In an ideal noise-free case, given the normalized image coordinates of the  $i$ -th correspondence on the two images, say  $\mathbf{y}_i^h$  and  $\mathbf{z}_i^h$ , the epipolar constraint yields the basic equation for the essential matrix:

$$\mathbf{z}_i^{h\top} \mathbf{E} \mathbf{y}_i^h = 0. \quad (1)$$

Most literature estimates the essential matrix by minimizing the algebraic error originating from (1) [11]–[15]. There are also some works minimizing geometric errors alternatively, such as the projection error [1], [16], [17]. No matter what formulation is adopted, the resulting optimization problem is nonconvex since the set of essential matrices is a nonconvex manifold. Some works devised Gauss-Newton (GN) iterations on manifold to guarantee that the estimate at each iteration is an essential matrix [13], [18], [19]. These local search methods require a good initial value, otherwise, they will converge to local minima. A more prevalent idea is conducting relaxation, e.g., semidefinite relaxation (SDR) [11], [14], [20] and direct linear transformation (DLT) [5], [21] to obtain an optimization problem whose global minimizer can be obtained. Nevertheless, the global minimizer of the modified problem is not necessarily that of the original problem. In short, the global solution to the optimization problem over the essential matrix manifold is still an open problem.

It should be noted that most of the literature sets out from the epipolar constraint (1), which is not the original measurement model. As a result, the formulated optimization problem is generally not optimal in the maximum

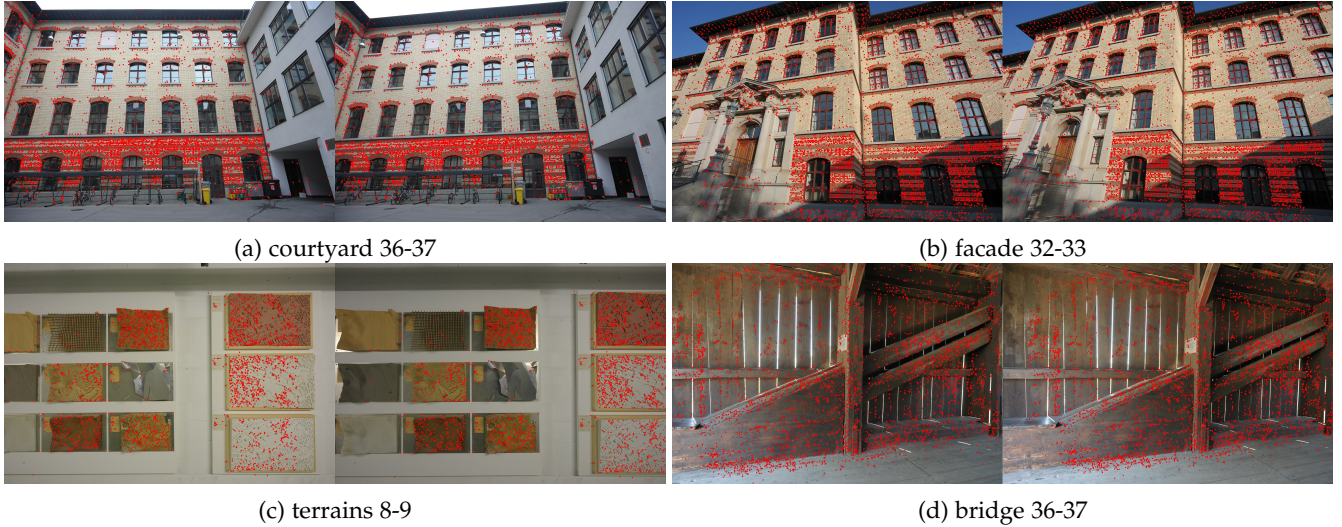


Figure 1: Four image pairs from the ETH3D dataset [22]. The red points are matched feature points. Each image pair has thousands of point correspondences.

likelihood (ML) sense. This will be explicitly discussed in Section 4. From the estimation theory, we know that the ML estimator is statistically optimal in the sense that under some regularity conditions, it is *consistent* and *asymptotically statistically-efficient* [23]. Here, *consistent* means that with the increase of point number, the estimate converges to the true value, and *asymptotically statistically-efficient* denotes that as the point number becomes sufficiently large, the mean squared error (MSE) of the estimate reaches the theoretical lower bound — Cramer-Rao bound (CRB)<sup>1</sup>. Thus, a more appropriate method should take the original measurement model and measurement noises into account and formulate an ML problem. Similar to the existing formulations, the ML problem is nonconvex, and finding its global solution is a challenging task.

In this paper, we utilize the rotation matrix and normalized translation vector, instead of the compound essential matrix, to obtain the original measurement model — a noise-contaminated function between matched 2D points, based on which the ML problem is formulated. For the nonconvex ML problem, we propose a two-step algorithm that can optimally solve it in the asymptotic case where the number of point correspondences is large. In other words, the obtained estimator is consistent and asymptotically statistically-efficient. It is noteworthy to see that in some texture-rich scenarios, one can obtain a large number of feature correspondences. For instance, as shown in Fig. 1, in the public dataset of ETH3D [22], there may exist thousands of point correspondences in an image pair. With abundant points, our algorithm achieves higher estimation accuracy compared with state-of-the-art algorithms. Actually, according to the results of simulations and real image tests, our algorithm begins to show its advantage when the point number reaches the order of hundreds. Besides estimation accuracy, time complexity is another important metric to appraise an algorithm, especially in the case of a large number of feature points. Since a closed-form solution is

1. We use statistically-efficient to distinguish from computationally-efficient which describes an algorithm that has low time complexity.

available in the first step, and only a one-step GN iteration is executed in the second step, our algorithm is *computationally efficient* — it has linear time complexity overall and has the capacity of real-time implementation even when the point number reaches the order of thousands. To summarize, the main contributions of this paper are listed as follows:

- (i). We derive the analytic expression between 2D point correspondences, see (6). The expression is the original measurement model, which is a function of the rotation matrix and normalized translation, instead of the essential matrix. Based on the measurement model, the statistically optimal ML problem is formulated.
- (ii). In the first step of our algorithm, we propose a novel consistent estimator of the measurement noise variance. It only involves calculating the maximum eigenvalue of a  $9 \times 9$  matrix. Based on the noise variance estimate, we perform bias elimination and eigenvalue decomposition, obtaining consistent estimates of the rotation matrix and normalized translation.
- (iii). In the second step of our algorithm, we take the consistent estimates as the initial value and devise the GN iterations on  $SO(3)$  (for the rotation matrix) and 2-sphere (for the normalized translation). Moreover, we prove that only a one-step of GN iteration is sufficient to achieve the same asymptotic property as the ML estimate, i.e., the MSE asymptotically reaches the CRB.
- (iv). We conduct extensive experiments with both synthetic data and real images. The results show that our proposed algorithm outperforms state-of-the-art ones in terms of estimation accuracy and CPU time when the point number reaches the order of hundreds. The open source code is available at [https://github.com/LIAS-CUHKSZ/epipolar\\_eval](https://github.com/LIAS-CUHKSZ/epipolar_eval).

The remainder of the paper is organized as follows. In Section 2, we review the related work on camera motion estimation. In Section 3, we introduce some notations and necessary preliminaries. In Section 4, we derive the original measurement model and formulate the ML problem. In Section 5, we estimate the variance of measurement noises

and propose a consistent estimator. In Section 6, we refine the consistent estimate via GN iterations on  $\text{SO}(3)$  and the 2-sphere. Experiment results are presented in Section 7, followed by conclusions in Section 8.

## 2 RELATED WORK

In CME, the epipolar geometry constraint yields a linear equation of the essential matrix, as shown in (1). Given an essential matrix, the rotation and normalized translation can be recovered via singular value decomposition [1]. Thus, most of the literature estimates the essential matrix in CME. The rotation matrix and translation vector have three degrees of freedom each. The essential matrix loses one degree of freedom because of scale ambiguity. Hence, it has in total five degrees of freedom, and at least five points are needed to estimate it [6], [24]–[27], which is called the minimal case. It is noteworthy to see that the normalized image coordinates are used in estimating the essential matrix. If the pixel coordinates are utilized, one can adopt eight-point solvers [5], [28] to estimate the fundamental matrix, which along with the intrinsic matrix can further recover the essential matrix. The above algorithms fall into the scope of fixed-point solvers. They are sensitive to measurement noises and usually need to be embedded in a RANSAC framework to enhance robustness [11], [29].

More literature studies arbitrary-point solvers since they can make full use of the whole measurements. Note that the set of essential matrices is nonconvex. Hence, the optimization problems over this set are nonconvex, and how to find a global solution is still an open problem. Some works devised local iterations on the manifold of essential matrices to seek a nearby stationary solution [13], [18], [19], [30]. In these works, the essential matrix manifold is characterized by different formulations, leading to distinct performances and convergence rates. Ma *et al.* [18] took the eight-point estimate as the initial value and proposed a Riemannian-Newton algorithm to solve the structure-from-motion problem. Helmke *et al.* [13] improved the convergence property and reduced the computational cost by proposing Gauss-Newton-type algorithms. Tron and Daniilidis [19] characterized the space of essential matrices as a quotient manifold that takes the symmetric role played by the two views and the geometric peculiarities of the epipolar constraint into account. We remark that the local iterative methods are sensitive to initial values. Without a good initial value, they can only converge to local minima.

Instead of local searching, many works focus on globally optimal solvers. Branch and bound (BnB) methods, which explore the whole optimization space, were utilized in [16], [31]. They achieve global optima but are computationally inefficient — exponential time in the worst case. Problem relaxation is a widely adopted idea for devising global solvers. The polynomial optimization problems established over the essential matrix manifold can be reformulated as QCQP problems, which can be further relaxed into semidefinite programming (SDP) problems via Shor’s relaxation [32]. Although the SDP problems can be globally solved in polynomial time with off-the-shelf tools, their global minima generally do not coincide with that of the original problem. Therefore, recently, some works characterized the theoretical

properties of the proposed SDP solvers. In [14], [33], certifiable relative pose solvers were proposed whose optimality w.r.t. the original problem can be certified a posteriori. Zhao [11] also presented a certifiable SDP-based solver. In addition, the tightness of the SDR relaxation was proved when the noise intensity is small.

To summarize, most of the literature estimates the essential matrix that encodes rotation and translation information instead of directly optimizing the rotation matrix and normalized translation vector. In addition, due to the nonconvexity of the essential matrix manifold, the global solution to the resulting problem is still an open problem. In the rest of this paper, we set out from the original measurement model and formulate an optimization problem in the ML sense, which optimizes directly over the rotation matrix and normalized translation vector. Moreover, we propose an asymptotically optimal two-step algorithm that can optimally solve the formulated nonconvex problem when the point number is large.

## 3 PRELIMINARIES

To facilitate the readability of the subsequent technical part, in this section, we present some notations and preliminaries in probability and statistics, rigid transformation, and the essential matrix.

### 3.1 Notations

We use bold lowercase letters to denote vectors, e.g.,  $\mathbf{x}$ ,  $\mathbf{y}$ ,  $\mathbf{z}$ , and bold uppercase letters for matrices, e.g.,  $\mathbf{X}$ ,  $\mathbf{Y}$ ,  $\mathbf{Z}$ . The identity matrix of size  $n$  is represented as  $\mathbf{I}_n$ . We denote the all-zeros vector of size  $n$  as  $\mathbf{0}_n$ , and the all-zeros matrix of size  $n \times n$  as  $\mathbf{O}_n$ . The all-ones vector of size  $n$  is  $\mathbf{1}_n$ . We use  $\mathbf{x} \geq \mathbf{y}$  to denote the element-wise inequality. The operation  $\otimes$  denotes the Kronecker product. For a vector  $\mathbf{x}$ ,  $\|\mathbf{x}\|$  denotes its  $\ell_2$ -norm. Given a matrix  $\mathbf{X}$ ,  $\|\mathbf{X}\|_F$  denotes its Frobenius norm,  $\text{tr}(\mathbf{X})$  represents its trace, and  $\text{vec}(\mathbf{X})$  yields a vector by concatenating the columns of  $\mathbf{X}$ . If  $\mathbf{X}$  has real eigenvalues, then  $\lambda_{\min}(\mathbf{X})$  and  $\lambda_{\max}(\mathbf{X})$  denote the minimum and maximum eigenvalues of  $\mathbf{X}$ , respectively. For a quantity  $\mathbf{x}$  corrupted by noise, we use  $\mathbf{x}^o$  to denote its noise-free counterpart.

### 3.2 Preliminaries in probability and statistics

**Convergence in probability.** We use  $\hat{\theta}_m \xrightarrow{p} \theta^o$  to denote that  $\hat{\theta}_m$  converges to  $\theta^o$  in probability, i.e., for any  $\varepsilon > 0$ ,

$$\lim_{m \rightarrow \infty} P(|\hat{\theta}_m - \theta^o| \geq \varepsilon) = 0.$$

In addition, the notation  $\Delta \hat{\theta}_m = o_p(a_m)$  means that the sequence  $\Delta \hat{\theta}_m/a_m$  converges to  $\mathbf{0}$  in probability.

**Stochastic boundedness.** The notation  $\Delta \hat{\theta}_m = O_p(a_m)$  means that the sequence  $\Delta \hat{\theta}_m/a_m$  is stochastically bounded. That is, for any  $\varepsilon > 0$ , there exists a finite  $M$  and a finite  $N$  such that for any  $m > M$ ,

$$P(|\Delta \hat{\theta}_m/a_m| > N) < \varepsilon.$$

**$\sqrt{m}$ -consistent estimate.** If  $\hat{\theta}_m$  is a  $\sqrt{m}$ -consistent estimate of  $\theta^o$ , then

$$\hat{\theta}_m - \theta^o = O_p(1/\sqrt{m}).$$

This notion includes two implications: The estimate  $\hat{\theta}_m$  is consistent — it converges to  $\theta^o$  in probability; The convergence rate is  $1/\sqrt{m}$ .

**(Asymptotically) unbiased estimate.** The bias of an estimate  $\hat{\theta}_m$  is equal to its expectation minus the true value, i.e.,  $\text{Bias}(\hat{\theta}_m) = \mathbb{E}[\hat{\theta}_m] - \theta^o$ . If  $\text{Bias}(\hat{\theta}_m) = 0$ , we call  $\hat{\theta}_m$  an unbiased estimate of  $\theta^o$ . In particular, if  $\lim_{m \rightarrow \infty} \text{Bias}(\hat{\theta}_m) = 0$ , we call  $\hat{\theta}_m$  an asymptotically unbiased estimate. It is noteworthy to see that an asymptotically unbiased estimate  $\hat{\theta}_m$  may not necessarily be unbiased when  $m$  is finite.

**(Asymptotically) efficient estimate.** An unbiased estimate  $\hat{\theta}_m$  is said to be efficient if the trace of its covariance is equal to the theoretical lower bound — CRB, i.e.,  $\text{tr}(\text{cov}(\hat{\theta}_m)) = \text{CRB}$ . In particular,  $\hat{\theta}_m$  is called asymptotically efficient if it is asymptotically unbiased, and  $\lim_{m \rightarrow \infty} \text{tr}(\text{cov}(\hat{\theta}_m)) = \text{CRB}$ .

### 3.3 Rigid transformation and the essential matrix

The (proper) rigid transformations, or said relative poses, include rotations and translations. The rotation can be characterized by a rotation matrix  $\mathbf{R}$ . Specifically, in the 3D Euclidean space, rotation matrices belong to the special orthogonal group

$$\text{SO}(3) = \{\mathbf{R} \in \mathbb{R}^{3 \times 3} \mid \mathbf{R}^\top \mathbf{R} = \mathbf{I}_3, \det(\mathbf{R}) = 1\}.$$

The translation is depicted by a vector  $\mathbf{t} \in \mathbb{R}^3$ . Suppose the relative pose of the second frame w.r.t. the first frame is  $(\mathbf{R}, \mathbf{t})$ , and the coordinates of a 3D point in the second frame is  $\mathbf{x}$ . Then the coordinates of the point in the first frame is  $\mathbf{R}\mathbf{x} + \mathbf{t}$ .

Given a vector  $\mathbf{t} = [t_1 \ t_2 \ t_3]^\top \in \mathbb{R}^3$ , the “hat” function  $\mathbf{t}^\wedge$  generates the following skew-symmetric matrix

$$\mathbf{t}^\wedge = \begin{bmatrix} 0 & -t_3 & t_2 \\ t_3 & 0 & -t_1 \\ -t_2 & t_1 & 0 \end{bmatrix}.$$

In epipolar geometry, the essential matrix is given as

$$\mathbf{E} = \mathbf{t}^\wedge \mathbf{R}. \quad (2)$$

In the noise-free case, the epipolar constraint is depicted by equation (1) in Section 1.

As mentioned previously, the distance of the translation  $\mathbf{t}$  cannot be identified given an image pair, hence we are interested in the normalized translation  $\bar{\mathbf{t}}$ , which belongs to the 2-sphere

$$S^2 = \{\bar{\mathbf{t}} \in \mathbb{R}^3 \mid \|\bar{\mathbf{t}}\| = 1\}.$$

This derives the set of normalized essential matrices

$$\mathcal{M}_E = \{\mathbf{E} \mid \mathbf{E} = \bar{\mathbf{t}}^\wedge \mathbf{R}, \exists \mathbf{R} \in \text{SO}(3), \bar{\mathbf{t}} \in S^2\}.$$

## 4 ML PROBLEM FORMULATION FROM ORIGINAL MEASUREMENT MODEL

We consider the pinhole camera model and assume the intrinsic matrices of cameras are known. The two-view geometry is shown in Fig. 2. We use  $\mathbf{x}_i = [x_{i1} \ x_{i2} \ x_{i3}]^\top \in \mathbb{R}^3, i \in \{1, \dots, m\}$  to denote the coordinates of the  $i$ -th 3D point in the world frame. Its 2D projections on the image planes are  $\mathbf{y}_i = [y_{i1} \ y_{i2}]^\top \in \mathbb{R}^2$  and  $\mathbf{z}_i = [z_{i1} \ z_{i2}]^\top \in \mathbb{R}^2$ .

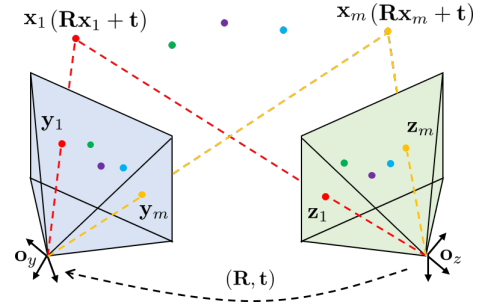


Figure 2: Two-view geometry.

Given the intrinsic matrices of cameras, we can use normalized image coordinates to represent points in the image, i.e., the focal length is set to be 1. The homogeneous normalized image coordinates of  $\mathbf{y}_i$  and  $\mathbf{z}_i$  are denoted as  $\mathbf{y}_i^h = [\mathbf{y}_i^\top \ 1]^\top$  and  $\mathbf{z}_i^h = [\mathbf{z}_i^\top \ 1]^\top$ , respectively. without loss of generality, we take the first camera frame as the world frame. Then, the projection model for the first camera is

$$\mathbf{y}_i = \frac{\mathbf{W}\mathbf{x}_i}{\mathbf{e}_3^\top \mathbf{x}_i} = \begin{bmatrix} x_{i1}/x_{i3} \\ x_{i2}/x_{i3} \end{bmatrix}, \quad (3)$$

where  $\mathbf{e}_i$  denotes the unit vector whose  $i$ -th element is 1, and  $\mathbf{W} = [\mathbf{e}_1 \ \mathbf{e}_2]^\top$ . Let  $\mathbf{R}$  and  $\mathbf{t}$  be the rotation matrix and translation vector of the first camera w.r.t. the second one. Then, the coordinates of the  $i$ -th 3D point in the second camera frame is  $\mathbf{R}\mathbf{x}_i + \mathbf{t}$ , and the corresponding projection model is

$$\mathbf{z}_i = \frac{\mathbf{W}(\mathbf{R}\mathbf{x}_i + \mathbf{t})}{\mathbf{e}_3^\top (\mathbf{R}\mathbf{x}_i + \mathbf{t})}. \quad (4)$$

Recall that only the direction of  $\mathbf{t}$  can be identified, while its scale cannot. If  $\mathbf{t} = \mathbf{0}$ , its direction becomes arbitrary, and the identifiability condition fails. Therefore, for the two camera centers, we make the following assumption:

**Assumption 1.** *The centers of the two cameras do not coincide, i.e.,  $\|\mathbf{t}\| \neq 0$ .*

Assumption 1 serves as a necessary condition to estimate the translation (up to a scale). When  $\|\mathbf{t}\| = 0$ , the direction of  $\mathbf{t}$  cannot be identified, and the CRB goes to infinity, see Fig. 5. In this case, the homography matrix should be used instead of the essential matrix. Apart from Assumption 1, we also need an assumption on the spatial distribution of 3D points and the two camera centers to ensure the global identifiability of the relative pose. Before that, we will introduce the notion of *ruled quadric surfaces*. A quadric is a surface in the projective space  $\mathbb{P}^3$  and is defined to be the set of points  $\mathbf{x}^h$  such that  $\mathbf{x}^{h\top} \mathbf{Q} \mathbf{x}^h = 0$ , where  $\mathbf{Q}$  is a symmetric  $4 \times 4$  matrix. A ruled quadric surface is a quadric surface that contains a straight line. It includes a hyperboloid of one sheet, a cone, two (intersecting) planes, a single plane, and a single line [1].

**Assumption 2.** *The 3D points  $\{\mathbf{x}_i\}_{i=1}^m$  and the two camera centers  $\mathbf{o}_y$  and  $\mathbf{o}_z$  do not lie on a ruled quadric surface.*

Assumption 2 ensures that there do not exist two different configurations of  $\{\mathbf{x}_i\}_{i=1}^m, \mathbf{R}$  and  $\mathbf{t}$  (up to a scale) that have the same projections  $\{\mathbf{y}_i\}_{i=1}^m$  and  $\{\mathbf{z}_i\}_{i=1}^m$  [1]. In other words,  $\mathbf{R}$  can be uniquely identified, and  $\mathbf{t}$  can be uniquely

identified up to a scale. A complete enumeration of the types of placement on a ruled quadric surface is given in [1, Result 22.11]. In general, the feature points are randomly distributed and will not concentrate on any ruled quadric surface. The most likely adverse scenario is that feature points concentrate on a man-made plane, e.g., a wall. In this case, CME algorithms may have unstable performance, which will be shown in Section 7.

By combining (3) and (4), we obtain the following relationship between  $\mathbf{z}_i$  and  $\mathbf{y}_i$ :

$$\begin{aligned} \mathbf{z}_i &= \frac{\mathbf{W}(\mathbf{R}\mathbf{y}_i^h + \mathbf{t}/x_{i3})}{\mathbf{e}_3^\top (\mathbf{R}\mathbf{y}_i^h + \mathbf{t}/x_{i3})} \\ &= \frac{\mathbf{W}(\mathbf{R}\mathbf{y}_i^h + k_i \bar{\mathbf{t}})}{\mathbf{e}_3^\top (\mathbf{R}\mathbf{y}_i^h + k_i \bar{\mathbf{t}})}, \end{aligned} \quad (5)$$

where  $\bar{\mathbf{t}} = \mathbf{t}/\|\mathbf{t}\|$ , and  $k_i = \|\mathbf{t}\|/x_{i3}$ . It is well-recognized that only the direction of  $\mathbf{t}$ , i.e.,  $\bar{\mathbf{t}}$  can be estimated from two-view geometry, while the length of  $\mathbf{t}$ , i.e.,  $\|\mathbf{t}\|$  cannot be recovered [1]. This forms the motivation that we use  $\bar{\mathbf{t}}$  in measurement model (5).

Note that the measurement equation (5) models the noise-free relationship between  $\mathbf{z}_i$  and  $\mathbf{y}_i$ . In real applications, there exist measurement noises due to, for example, a nonideal pinhole model, the inaccuracy of intrinsic matrix calibration, the spatial inconsistency of feature points, etc. Hence, the real measurement model should be

$$\mathbf{z}_i = \frac{\mathbf{W}(\mathbf{R}\mathbf{y}_i^h + k_i \bar{\mathbf{t}})}{\mathbf{e}_3^\top (\mathbf{R}\mathbf{y}_i^h + k_i \bar{\mathbf{t}})} + \epsilon_i, \quad (6)$$

where  $\epsilon_i$  is the measurement noise.

**Assumption 3.** *The measurement noises  $\epsilon_i \sim \mathcal{N}(0, \sigma^2 \mathbf{I}_2)$ ,  $i = 1, \dots, m$  are independent and identically distributed (i.i.d.) with unknown variance  $\sigma^2$ .*

The i.i.d. Gaussian noise assumption has been widely adopted in estimations in computer vision, e.g., [34]–[36]. We remark that when  $\mathbf{y}_i$  and  $\mathbf{z}_i$  correspond to the same  $\mathbf{x}_i$ , model (6) essentially characterizes the “error in one image” case that is frequently assumed in [1]. Note that in (6), we have established the relationship between  $\mathbf{z}_i$  and  $\mathbf{y}_i$ , and the measurement noise is in its most natural form. Hence, we call (6) the *original measurement model* and will use it to construct the ML problem. Specifically, the residual is

$$\mathbf{r}_i = \mathbf{z}_i - \frac{\mathbf{W}(\mathbf{R}\mathbf{y}_i^h + k_i \bar{\mathbf{t}})}{\mathbf{e}_3^\top (\mathbf{R}\mathbf{y}_i^h + k_i \bar{\mathbf{t}})}. \quad (7)$$

Given point correspondences  $\{(\mathbf{y}_i, \mathbf{z}_i)\}_{i=1}^m$ , by utilizing the least-squares (LS) criterion to model (6), we obtain the following LS problem:

$$\underset{\mathbf{R}, \bar{\mathbf{t}}, \{k_i\}}{\text{minimize}} \quad \frac{1}{m} \sum_{i=1}^m \|\mathbf{r}_i\|^2 \quad (8a)$$

$$\text{subject to} \quad \mathbf{R} \in \text{SO}(3) \quad (8b)$$

$$\bar{\mathbf{t}} \in S^2 \quad (8c)$$

$$k_i > 0, i = 1, \dots, m. \quad (8d)$$

Given Assumption 3, the LS problem (8) is also the ML problem. The global solution to the ML problem (8) (called the ML estimate) is consistent and asymptotically

statistically-efficient. However, the ML problem (8) is non-convex, and finding its global solution is nontrivial. When using local iterations, e.g., the GN algorithm, an appropriate initial solution is needed, otherwise, it will converge to local minima. In the next section, we will propose a consistent estimator. The resulting consistent solution serves as a good initial value in the sense that GN iterations converge to the global minimizer of (8) in the asymptotic case.

We note that most of the literature adopts the algebraic error  $(\mathbf{z}_i^{h\top} \mathbf{E} \mathbf{y}_i^h)^2$  which stems from the basic equation (1) of the essential matrix and formulates the following problem [11]–[13]:

$$\underset{\mathbf{E}}{\text{minimize}} \quad \frac{1}{m} \sum_{i=1}^m \left( \mathbf{z}_i^{h\top} \mathbf{E} \mathbf{y}_i^h \right)^2 \quad (9a)$$

$$\text{subject to} \quad \mathbf{E} \in \mathcal{M}_E. \quad (9b)$$

We now discuss the difference between formulations (8) and (9) by taking measurement noises into account. Let  $\epsilon_i^h = [\epsilon_i^\top \ 0]^\top$  denote the homogeneous noise. Based on epipolar geometry constraint, we obtain the equation  $(\mathbf{z}_i^h - \epsilon_i^h)^\top \mathbf{E} \mathbf{y}_i^h = 0$ , i.e.,

$$0 = \mathbf{z}_i^{h\top} \mathbf{E} \mathbf{y}_i^h - \eta_i, \quad (10)$$

where  $\eta_i = \epsilon_i^{h\top} \mathbf{E} \mathbf{y}_i^h$  is the new noise term. Then, one can find that problem (9) is essentially obtained by utilizing the LS criterion to (10). We remark that there are two main differences between formulations (8) and (9). First, the original noise terms  $\epsilon_i$ 's in model (6) have the same variance, hence, in (8), we adopt the unweighted LS formulation. However, the new noise term  $\eta_i$  is a function of  $\mathbf{y}_i^h$ , making  $\eta_i$ 's have different variances. Therefore, the weighted squared residual  $(\mathbf{z}_i^{h\top} \mathbf{E} \mathbf{y}_i^h)^2 / \sigma_i^2$  ( $\sigma_i^2$  is the variance of  $\eta_i$ ) should have been used in (9) to yield a minimum estimation covariance. Unfortunately,  $\sigma_i^2$  is not available since  $\eta_i$  is a function of the unknown matrix  $\mathbf{E}$ . Second, a more severe issue is that the regressor  $\mathbf{z}_i^{h\top} \mathbf{E} \mathbf{y}_i^h$  in (10) contains  $\epsilon_i$  and is correlated with the noise term  $\eta_i$ . According to estimation theory, this will make the resulting estimator not asymptotically unbiased [37]. In other words, the global solution to (9) is not consistent. Note that in the original model (6), the regressor  $\frac{\mathbf{W}(\mathbf{R}\mathbf{y}_i^h + k_i \bar{\mathbf{t}})}{\mathbf{e}_3^\top (\mathbf{R}\mathbf{y}_i^h + k_i \bar{\mathbf{t}})}$  is not correlated with the noise term  $\epsilon_i$ . This serves as a prerequisite for the consistency of the ML estimate. In summary, the global solution to (8) (the ML estimate) has the statistical property of consistency and asymptotic efficiency, while the global solution to (10) has no theoretical guarantee.

## 5 CONSISTENT ESTIMATOR DESIGN

In this section, we focus on the design of a  $\sqrt{m}$ -consistent estimator. The resulting estimates  $\hat{\mathbf{R}}_m$  and  $\hat{\mathbf{t}}_m$  satisfy

$$\hat{\mathbf{R}}_m - \mathbf{R}^o = O_p(1/\sqrt{m}), \quad \hat{\mathbf{t}}_m - \bar{\mathbf{t}}^o = O_p(1/\sqrt{m}), \quad (11)$$

where  $\mathbf{R}^o$  and  $\bar{\mathbf{t}}^o$  are ground truth. The design consists of two procedures: First, we provide a consistent estimate of noise variance by calculating the maximum eigenvalue of a  $9 \times 9$  matrix; We then execute bias elimination based on the estimate of noise variance and perform eigendecomposition to obtain a consistent solution.

## 5.1 Consistent noise variance estimation

Regarding an estimator with finite variance, asymptotic unbiasedness is a necessary condition for consistency [37]. On the one hand, in nonlinear nonconvex optimization, estimators obtained by relaxation are usually biased, even in the asymptotic case. On the other hand, the bias of an estimator is generally a function of the variance of measurement noises. Therefore, noise variance estimation is a prerequisite for bias elimination and the construction of a consistent solution. Let  $\mathbf{L}_i = \mathbf{y}_i^{h\top} \otimes \mathbf{I}_3 \in \mathbb{R}^{3 \times 9}$  and  $\boldsymbol{\theta} = \text{vec}(\mathbf{E}) \in \mathbb{R}^9$ , we can rewrite (10) as

$$0 = \mathbf{z}_i^{h\top} \mathbf{L}_i \boldsymbol{\theta} - \eta_i. \quad (12)$$

By stacking (12) for all  $i \in \{1, \dots, m\}$ , we obtain the matrix form:

$$\mathbf{0} = \mathbf{A}_m \boldsymbol{\theta} - \boldsymbol{\eta}_m, \quad (13)$$

where

$$\mathbf{A}_m = \begin{bmatrix} \mathbf{z}_1^{h\top} \mathbf{L}_1 \\ \vdots \\ \mathbf{z}_m^{h\top} \mathbf{L}_m \end{bmatrix}, \quad \boldsymbol{\eta}_m = \begin{bmatrix} \eta_1 \\ \vdots \\ \eta_m \end{bmatrix}.$$

Define

$$\mathbf{Q}_m = \frac{\mathbf{A}_m^\top \mathbf{A}_m}{m} \quad (14)$$

and

$$\mathbf{S}_m = \mathbf{Y}^h \otimes \mathbf{W}^h \quad (15)$$

where  $\mathbf{Y}^h = \sum_{i=1}^m \mathbf{y}_i^h \mathbf{y}_i^{h\top} / m$  and  $\mathbf{W}^h = [\mathbf{W}^\top \mathbf{0}_3]^\top$ . The following theorem gives a consistent estimate of the variance  $\sigma^2$  of the measurement noises  $\epsilon_i$ 's.

**Theorem 1.** *Let  $\hat{\sigma}_m^2 = 1/\lambda_{\max}(\mathbf{Q}_m^{-1} \mathbf{S}_m)$ . Then, under Assumptions 1-3,  $\hat{\sigma}_m^2$  is a  $\sqrt{m}$ -consistent estimate of  $\sigma^2$ .*

The proof is presented in Appendix A.

## 5.2 Bias elimination and eigendecomposition

With the  $\sqrt{m}$ -consistent estimate of noise variance given in Theorem 1, we are ready to propose a consistent estimator of the essential matrix  $\mathbf{E}$ . With the consistent estimate of  $\mathbf{E}$ , we can further recover the consistent estimates of  $\mathbf{R}$  and  $\bar{\mathbf{t}}$ . The consistent estimator is derived based on (13) and is tightly related to the classic 8-point algorithm [5]. The 8-point algorithm optimally solves the problem

$$\underset{\boldsymbol{\theta}}{\text{minimize}} \quad \|\mathbf{A}_m \boldsymbol{\theta}\|^2 \quad (16a)$$

$$\text{subject to} \quad \|\boldsymbol{\theta}\| = 1. \quad (16b)$$

Denote the SVD of  $\mathbf{A}_m$  as  $\mathbf{A}_m = \mathbf{U} \mathbf{D} \mathbf{V}^\top$ . Then, the singular vector corresponding to the smallest singular value of  $\mathbf{A}_m$ , i.e., the last column of  $\mathbf{V}$  is the global minimizer of problem (16). It can be verified that this is equivalent to finding the eigenvector corresponding to the smallest eigenvalue of  $\mathbf{Q}_m$  (Recall that  $\mathbf{Q}_m = \mathbf{A}_m^\top \mathbf{A}_m / m$ ). Although the formulation (16) arose from the 8-point problem, it is essentially a constrained least-squares formulation of (13) and can be used in arbitrary point number  $m$ .

To construct a consistent estimator of  $\boldsymbol{\theta}$  (i.e.,  $\mathbf{E}$  since  $\boldsymbol{\theta} = \text{vec}(\mathbf{E})$ ), first, we consider the noise-free problem

$$\underset{\boldsymbol{\theta}}{\text{minimize}} \quad \|\mathbf{A}_m^o \boldsymbol{\theta}\|^2 \quad (17a)$$

$$\text{subject to} \quad \|\boldsymbol{\theta}\| = 1. \quad (17b)$$

The following lemma characterizes the solutions of (17).

**Lemma 1.** *Given Assumption 2, the optimal solutions of (17) equal the true  $\boldsymbol{\theta}^o = \text{vec}(\bar{\mathbf{t}}^o \wedge \mathbf{R}^o)$  up to a scale.*

*Proof.* The proof is direct from Theorem 22.9 [1], which states that under Assumption 2, there exists a unique essential matrix  $\mathbf{E}$  up to a scale that exactly coincides with  $\{\mathbf{y}_i, \mathbf{z}_i^o\}_{i=1}^m$ . Since the constraint (17b) is equivalent to  $\|\mathbf{E}\|_F = 1$ , problem (17) has two optimal solutions: one is  $\boldsymbol{\theta}^o / \sqrt{2}$ , and the other is  $-\boldsymbol{\theta}^o / \sqrt{2}$ . Both solutions achieve a 0 value of the objective function (17a).  $\square$

As noted before, the unit eigenvectors associated with the smallest eigenvalue of  $\mathbf{Q}_m^o$  are the optimal solutions to (17). However, as the noise-free counterpart of  $\mathbf{Q}_m$ ,  $\mathbf{Q}_m^o$  is unavailable in practice. One natural idea is to eliminate the bias between  $\mathbf{Q}_m$  and  $\mathbf{Q}_m^o$  in the asymptotic case, and the bias-eliminated quantity  $\mathbf{Q}_m^{\text{BE}}$  converges to  $\mathbf{Q}_m^o$ . Then, we can calculate the eigenvectors of  $\mathbf{Q}_m^{\text{BE}}$  to obtain a consistent estimate of  $\boldsymbol{\theta}$ . Note that we can obtain a  $\sqrt{m}$ -consistent estimate  $\hat{\sigma}_m^2$  of  $\sigma^2$ . Let

$$\mathbf{Q}_m^{\text{BE}} = \mathbf{Q}_m - \hat{\sigma}_m^2 \mathbf{S}_m. \quad (18)$$

From (26) in Appendix A, we have

$$\mathbf{Q}_m^{\text{BE}} = \mathbf{Q}_m^o + O_p(1/\sqrt{m}). \quad (19)$$

The following theorem gives a  $\sqrt{m}$ -consistent estimate of  $\boldsymbol{\theta}^o$ .

**Theorem 2.** *One of the unit eigenvectors associated with  $\lambda_{\min}(\mathbf{Q}_m^{\text{BE}})$  is a  $\sqrt{m}$ -consistent estimate of  $\boldsymbol{\theta}^o / \sqrt{2}$ .*

*Proof.* From the proof of Lemma 1, we know that one of the unit eigenvectors associated with  $\lambda_{\min}(\mathbf{Q}_m^o)$  equals  $\boldsymbol{\theta}^o / \sqrt{2}$ . In addition,  $\mathbf{Q}_m^{\text{BE}}$  is a  $\sqrt{m}$ -consistent estimate of  $\mathbf{Q}_m^o$ , see (19), and eigenvector is a continuous function, which can preserve the property of  $\sqrt{m}$ -consistency. Thus, the proof is completed.  $\square$

Note that  $\boldsymbol{\theta} = \text{vec}(\mathbf{E})$ . The essential matrix can be obtained via inverse vectorization from  $\boldsymbol{\theta}$ . Given the estimate of the essential matrix, one can recover  $\bar{\mathbf{t}}$  and  $\mathbf{R}$  by the SVD. For the recovery of  $\bar{\mathbf{t}}$  and  $\mathbf{R}$ , there are two points worth mentioning [1]. First, the recovery result is invariant to scale, that is, for every  $k \neq 0$ ,  $k\mathbf{E}$  yields the same results as  $\mathbf{E}$ . Second, the recovery is not unique — it produces four pairs of  $(\mathbf{R}, \bar{\mathbf{t}})$ , and the correct one needs to be selected as the final estimate. The selection criterion is that the triangulated 3D points with the pair  $(\mathbf{R}, \bar{\mathbf{t}})$  should locate in front of two cameras. We utilize the `recoverPose` function in OpenCV to complete this task. Denote an arbitrary eigenvector associated with  $\lambda_{\min}(\mathbf{Q}_m^{\text{BE}})$  as  $\hat{\boldsymbol{\theta}}_m^{\text{BE}}$  and its recovery results as  $\hat{\bar{\mathbf{t}}}_m^{\text{BE}}$  and  $\hat{\mathbf{R}}_m^{\text{BE}}$ . Since  $\hat{\boldsymbol{\theta}}_m^{\text{BE}}$  is  $\sqrt{m}$ -consistent and the SVD is a continuous function, the following corollary is a straightforward extension of Theorem 2.

**Corollary 1.** *The solutions  $\hat{\bar{\mathbf{t}}}_m^{\text{BE}}$  and  $\hat{\mathbf{R}}_m^{\text{BE}}$  are  $\sqrt{m}$ -consistent estimates of  $\bar{\mathbf{t}}^o$  and  $\mathbf{R}^o$ .*

## 6 GAUSS-NEWTON ITERATIONS FOR ROTATION AND NORMALIZED TRANSLATION

Recall that our ultimate goal is to optimally solve the ML problem (8) in the asymptotic case. We achieve this via a two-step scheme. As shown in Section 5, in the first step, we have obtained consistent estimates  $\hat{\mathbf{t}}_m^{\text{BE}}$  and  $\hat{\mathbf{R}}_m^{\text{BE}}$ . It is noteworthy to see that although  $\hat{\mathbf{t}}_m^{\text{BE}}$  and  $\hat{\mathbf{R}}_m^{\text{BE}}$  own consistency, they are not optimal in the sense of minimum variance. Nonetheless, the consistency enables them to be a theoretically guaranteed initial value in the asymptotic case. As the number of points increases,  $\hat{\mathbf{t}}_m^{\text{BE}}$  and  $\hat{\mathbf{R}}_m^{\text{BE}}$  will converge into the attraction region of the global solution to (8), which ensures that GN iterations optimally solve (8). Therefore, in the second step, we conduct GN iterations to refine the consistent estimates  $\hat{\mathbf{t}}_m^{\text{BE}}$  and  $\hat{\mathbf{R}}_m^{\text{BE}}$ .

To let the refined solution converge to the ML estimate, GN iterations should be derived from the ML problem (8). However, this comes with two difficulties. First, in addition to  $\bar{\mathbf{t}}$  and  $\mathbf{R}$ , there are  $m$  unknown  $k_i$  in (8). If we involve updating  $k_i$ 's in the GN iterations, the Jacobian matrix  $\mathbf{J}$  has an expanding size as  $m$  increases, and calculating the inverse of  $\mathbf{J}^\top \mathbf{J}$  needs  $O(m^3)$  time complexity, which is computationally inefficient. Second, the GN iterations need to meet two constraints, that is, the rotation matrix belongs to  $\text{SO}(3)$ , and the normalized translation vector is on the 2-sphere. In what follows, we first eliminate  $k_i$ 's by resorting to the Karush-Kuhn-Tucker (KKT) conditions [32]. We then derive the GN iteration formulation on the  $\text{SO}(3)$  group and 2-sphere.

### 6.1 Variable elimination via KKT conditions

In this subsection, we express optimal  $k_i$ 's with  $\bar{\mathbf{t}}$  and  $\mathbf{R}$  by utilizing the KKT conditions. By doing so, the Jacobian matrix  $\mathbf{J}$  associated with only  $\bar{\mathbf{t}}$  and  $\mathbf{R}$  can be used, so the matrix  $\mathbf{J}^\top \mathbf{J}$  has a fixed size. Specifically, we denote the objective function of (8) as  $f_m$ . According to the KKT stationary condition, we have

$$\frac{\partial f_m}{\partial k_i} + \lambda_i = 0, \quad (20)$$

where  $\lambda_i$  is the Lagrange multiplier corresponding to  $k_i$ . In addition, the KKT complementary slackness condition requires that  $\lambda_i k_i = 0, i = 1, \dots, m$ . Next, we are going to show that  $\lambda_i = 0, i = 1, \dots, m$  in the asymptotic case. Let  $\mathbf{r}_i^o$  denote the residual in the noise-free case. We can decompose  $f_m$  as

$$\begin{aligned} f_m &= \frac{1}{m} \sum_{i=1}^m \|\mathbf{r}_i\|^2 \\ &= \frac{1}{m} \sum_{i=1}^m \|\mathbf{r}_i^o\|^2 + \underbrace{\frac{2}{m} \sum_{i=1}^m \epsilon_i^\top \mathbf{r}_i^o}_{\rightarrow 0} + \underbrace{\frac{1}{m} \sum_{i=1}^m \|\epsilon_i\|^2}_{\rightarrow 2\sigma^2} \\ &\rightarrow \underbrace{\frac{1}{m} \sum_{i=1}^m \|\mathbf{r}_i^o\|^2}_{:= f_m^o} + 2\sigma^2, \end{aligned}$$

where the third line is based on Lemma 3 in Appendix A. Note that  $f_m^o = 0$  when  $\mathbf{R}$ ,  $\bar{\mathbf{t}}$ , and  $k_i$ 's take true values.

Moreover, according to Theorem 22.9 [1], given Assumption 2, there does not exist a conjugate configuration of true values such that  $f_m^o = 0$ . In other words,  $f_m^o = 0$  only if  $k_i = \|\bar{\mathbf{t}}^o\|/x_{i3}^o > 0$ . Then, from the KKT complementary slackness condition  $\lambda_i k_i = 0$ , we obtain  $\lambda_i = 0, i = 1, \dots, m$ . The derivative of  $f_m$  w.r.t.  $k_i$  is

$$\frac{\partial f_m}{\partial k_i} = \frac{2\mathbf{r}_i^\top \mathbf{e}_3^\top \bar{\mathbf{t}} \mathbf{W} (\mathbf{R} \mathbf{y}_i^h + k_i \bar{\mathbf{t}}) - \mathbf{e}_3^\top (\mathbf{R} \mathbf{y}_i^h + k_i \bar{\mathbf{t}}) \mathbf{W} \bar{\mathbf{t}}}{m (\mathbf{e}_3^\top (\mathbf{R} \mathbf{y}_i^h + k_i \bar{\mathbf{t}}))^2}. \quad (21)$$

By combining (20) and  $\lambda_i = 0$ , we have  $\partial f_m / \partial k_i = 0$ . Hence, we can express optimal  $k_i$ 's with  $\bar{\mathbf{t}}$  and  $\mathbf{R}$  from (21). Here we omit the tedious derivation and directly give the result:

$$k_i = \frac{\mathbf{y}_i^{h\top} \mathbf{R}^\top \mathbf{C}_1 (\mathbf{I}_3 \otimes \bar{\mathbf{t}}) \mathbf{R} \mathbf{y}_i^h}{\bar{\mathbf{t}}^\top \mathbf{C}_2 (\mathbf{I}_3 \otimes \bar{\mathbf{t}}) \mathbf{R} \mathbf{y}_i^h}, \quad (22)$$

where

$$\mathbf{C}_1 = \begin{bmatrix} -\mathbf{e}_3^\top & \mathbf{0}_3^\top & z_{i1} \mathbf{e}_3^\top \\ \mathbf{0}_3^\top & -\mathbf{e}_3^\top & z_{i2} \mathbf{e}_3^\top \\ \mathbf{e}_1^\top & \mathbf{e}_2^\top & -(z_{i1} \mathbf{e}_1^\top + z_{i2} \mathbf{e}_2^\top) \end{bmatrix},$$

$$\mathbf{C}_2 = \begin{bmatrix} \mathbf{e}_3^\top & \mathbf{0}_3^\top & z_{i1} \mathbf{e}_3^\top - \mathbf{e}_1^\top \\ \mathbf{0}_3^\top & \mathbf{e}_3^\top & z_{i2} \mathbf{e}_3^\top - \mathbf{e}_2^\top \\ -z_{i1} \mathbf{e}_3^\top & -z_{i2} \mathbf{e}_3^\top & \mathbf{0}_3^\top \end{bmatrix}.$$

### 6.2 Gauss-Newton iterations on $\text{SO}(3)$ and 2-sphere

Since the GN algorithm is an extension of Newton's method, when the initial guess is near the minimum, the rate of its convergence can approach quadratic. Thanks to the  $\sqrt{m}$ -consistent property of  $\hat{\mathbf{R}}_m^{\text{BE}}$  and  $\hat{\mathbf{t}}_m^{\text{BE}}$ , when the point number  $m$  is large, they are sufficiently near the global minimum of the ML problem (8), and only a one-step GN iteration suffices to achieve the same asymptotic property (i.e., asymptotically statistically-efficient) as the ML estimate  $\hat{\mathbf{R}}_m^{\text{ML}}$  and  $\hat{\mathbf{t}}_m^{\text{ML}}$ , which will be formally stated in Theorem 3. Before that, we take  $\hat{\mathbf{R}}_m^{\text{BE}}$  and  $\hat{\mathbf{t}}_m^{\text{BE}}$  as the initial value and derive the one-step GN iteration.

Note that the rotation matrix belongs to  $\text{SO}(3)$ , and the normalized translation locates on the 2-sphere. Hence, we are going to derive the GN iteration formulation on  $\text{SO}(3)$  and 2-sphere. For the  $\text{SO}(3)$  constraint, given the initial estimate  $\hat{\mathbf{R}}_m^{\text{BE}} \in \text{SO}(3)$  and any  $\mathbf{s} \in \mathbb{R}^3$ , the matrix  $\hat{\mathbf{R}}_m^{\text{BE}} \exp(\mathbf{s}^\wedge)$  also belongs to  $\text{SO}(3)$ . Hence, we can update the unconstrained vector  $\mathbf{s}$  to guarantee the refined rotation matrix estimate is still in  $\text{SO}(3)$ . For the 2-sphere constraint, let

$$\alpha_0 = \sin^{-1} \left( \frac{\hat{t}_{m3}^{\text{BE}}}{\|\hat{\mathbf{t}}_m^{\text{BE}}\|} \right),$$

$$\beta_0 = \begin{cases} \tan^{-1} \left( \frac{\hat{t}_{m2}^{\text{BE}} / \hat{t}_{m1}^{\text{BE}}}{\hat{t}_{m2}^{\text{BE}} / \hat{t}_{m1}^{\text{BE}}} \right), & \text{if } \hat{t}_{m1}^{\text{BE}} > 0 \\ \tan^{-1} \left( \frac{\hat{t}_{m2}^{\text{BE}} / \hat{t}_{m1}^{\text{BE}}}{\hat{t}_{m2}^{\text{BE}} / \hat{t}_{m1}^{\text{BE}}} \right) + 180^\circ, & \text{if } \hat{t}_{m1}^{\text{BE}} < 0, \end{cases}$$

where we express  $\hat{\mathbf{t}}_m^{\text{BE}}$  as  $\hat{\mathbf{t}}_m^{\text{BE}} = [\hat{t}_{m1}^{\text{BE}} \ \hat{t}_{m2}^{\text{BE}} \ \hat{t}_{m3}^{\text{BE}}]^\top$ . Given any  $\alpha, \beta \in \mathbb{R}$ , the vector

$$\bar{\mathbf{t}}(\alpha, \beta) = \begin{bmatrix} \cos(\alpha_0 + \alpha) \cos(\beta_0 + \beta) \\ \cos(\alpha_0 + \alpha) \sin(\beta_0 + \beta) \\ \sin(\alpha_0 + \alpha) \end{bmatrix}$$

is still on the 2-sphere. Hence, we can update  $\alpha$  and  $\beta$  to refine the normalized translation estimate. Let  $\hat{\mathbf{s}}_m^{\text{GN}}$ ,  $\hat{\alpha}_m^{\text{GN}}$ , and  $\hat{\beta}_m^{\text{GN}}$  denote the results obtained by a one-step GN iteration. Then the refined rotation matrix and normalized translation vector are given as

$$\hat{\mathbf{R}}_m^{\text{GN}} = \hat{\mathbf{R}}_m^{\text{BE}} \exp(\hat{\mathbf{s}}_m^{\text{GN}^\wedge}), \quad \hat{\mathbf{t}}_m^{\text{GN}} = \bar{\mathbf{t}}(\hat{\alpha}_m^{\text{GN}}, \hat{\beta}_m^{\text{GN}}). \quad (23)$$

For the explicit derivation of  $\hat{\mathbf{s}}_m^{\text{GN}}$ ,  $\hat{\alpha}_m^{\text{GN}}$ , and  $\hat{\beta}_m^{\text{GN}}$ , one can refer to Appendix B.

**Theorem 3.** Denote the one-step GN iteration of the  $\sqrt{m}$ -consistent estimates  $\hat{\mathbf{R}}_m^{\text{BE}}$  and  $\hat{\mathbf{t}}_m^{\text{BE}}$  by  $\hat{\mathbf{R}}_m^{\text{GN}}$  and  $\hat{\mathbf{t}}_m^{\text{GN}}$ , respectively. Then,

$$\hat{\mathbf{R}}_m^{\text{ML}} - \hat{\mathbf{R}}_m^{\text{GN}} = o_p(1/\sqrt{m}), \quad \hat{\mathbf{t}}_m^{\text{ML}} - \hat{\mathbf{t}}_m^{\text{GN}} = o_p(1/\sqrt{m}).$$

The proof of Theorem 3 is presented in Appendix C.

By now we have introduced the whole algorithm. In summary, it mainly consists of three modules: noise variance estimation, consistent solution construction, and a one-step GN refinement. The proposed algorithm is summarized in Algorithm 1, where we denote it as CECME — consistent and asymptotically statistically-efficient camera motion estimator. We remark that our algorithm has significant advantages in the asymptotic case. In terms of estimation accuracy, owing to the  $\sqrt{m}$ -consistency of  $\hat{\mathbf{R}}_m^{\text{BE}}$  and  $\hat{\mathbf{t}}_m^{\text{BE}}$  obtained in the first step, only a one-step GN iteration in the second step will suffice to achieve the CRB asymptotically, which is also verified by our simulation results. We put the derivation of the CRB in Appendix D. In terms of time complexity, it can be verified that **Lines 1,5,6** in Algorithm 1 cost  $O(m)$  time, and **Lines 2,3,4** cost  $O(1)$  time. Therefore, the whole time complexity of CECME is  $O(m)$ , making it suitable for real-time implementation when the point number  $m$  is large. The experiment results in the following section will demonstrate the superiority (in terms of MSE and CPU time) of the proposed algorithm over state-of-the-art ones when the point number is large.

---

#### Algorithm 1 CECME

---

**Input:** Point correspondences  $\{(\mathbf{y}_i, \mathbf{z}_i)\}_{i=1}^m$ .

**Output:** The estimates of the rotation matrix  $\hat{\mathbf{R}}_m^{\text{GN}}$  and normalized translation vector  $\hat{\mathbf{t}}_m^{\text{GN}}$ .

- 1: Calculate the matrix  $\mathbf{Q}_m$  in (14) and  $\mathbf{S}_m$  in (15);
  - 2: Obtain noise variance estimate via  $\hat{\sigma}_m^2 = 1/\lambda_{\max}(\mathbf{Q}_m^{-1}\mathbf{S}_m)$ ;
  - 3: Calculate  $\mathbf{Q}_m^{\text{BE}} = \mathbf{Q}_m - \hat{\sigma}_m^2\mathbf{S}_m$ ;
  - 4: Set  $\hat{\boldsymbol{\theta}}_m^{\text{BE}}$  as an arbitrary eigenvector of  $\mathbf{Q}_m^{\text{BE}}$  associated with  $\lambda_{\min}(\mathbf{Q}_m^{\text{BE}})$ ;
  - 5: Recover  $\hat{\mathbf{t}}_m^{\text{BE}}$  and  $\hat{\mathbf{R}}_m^{\text{BE}}$  from  $\hat{\boldsymbol{\theta}}_m^{\text{BE}}$ ;
  - 6: Execute a one-step GN iteration shown in (23).
- 

## 7 EXPERIMENT

In this section, we conduct experiments on both synthetic data and real images. The classical or state-of-the-art methods compared with ours are

- 5pt: the five-point algorithm proposed by Nister [6]
- Eigen: the eigenvalue-based method proposed by Kneip and Lynen [31]

- SDP: the SDP-based method proposed by Zhao [11]
- GN-E: the GN iterations on the manifold of normalized essential matrices proposed by Helmke *et al.* [13]

We use open source codes for 5pt, Eigen, and SDP methods, and realize the GN-E method by ourselves. Note that Eigen and GN-E need an initial guess of the rotation matrix and essential matrix, respectively. We take the results of the 5pt solver as their inputs.

### 7.1 Experiment with synthetic data

In the simulation, the translation is set as  $[5 \ 5 \ 5]^\top$  cm, and the Euler angles are  $[20^\circ \ 20^\circ \ 20^\circ]^\top$ . The two cameras have the same intrinsic matrix, where the focal length is  $f_x = f_y = 800$  pixels (5 cm), and the size of the image plane is  $640 \times 480$  pixels. The principle point lies in the top-left corner of the image plane and the principle point offsets are  $u_0 = 320$  pixels and  $v_0 = 240$  pixels. For the generation of 3D points that are visible in both images, we first randomly generate 2D points in the first image and then endow them each with a random depth within  $[1, 5]$  m. Only the 3D points whose projection in the second camera is within its image plane are selected as valid ones. As noted in Assumption 3, the measurement is corrupted by a zero-mean Gaussian noise whose standard deviation is  $\sigma$  pixels.

The evaluation metric for estimation accuracy is mean squared error (MSE), which is defined as follows:

$$\text{MSE}_{\mathbf{R}} = \frac{1}{K} \sum_{k=1}^K \left\| \hat{\mathbf{R}}_k - \mathbf{R}^o \right\|_F^2, \\ \text{MSE}_{\bar{\mathbf{t}}} = \frac{1}{K} \sum_{k=1}^K \left\| \hat{\mathbf{t}}_k - \bar{\mathbf{t}}^o \right\|^2,$$

where  $\hat{\mathbf{R}}_k$  and  $\hat{\mathbf{t}}_k$  are the estimates obtained in the  $k$ -th Monte Carlo test, and  $K$  is the total number of Monte Carlo tests. We also present the bias of each estimator. The bias is given as

$$\Delta \mathbf{R} = \left| \frac{1}{K} \sum_{k=1}^K \hat{\mathbf{R}}_k - \mathbf{R}^o \right|, \quad \text{Bias}_{\mathbf{R}} = \sum_{i=1}^3 \sum_{j=1}^3 \Delta \mathbf{R}_{ij} \\ \Delta \bar{\mathbf{t}} = \left| \frac{1}{K} \sum_{k=1}^K \hat{\mathbf{t}}_k - \bar{\mathbf{t}}^o \right|, \quad \text{Bias}_{\bar{\mathbf{t}}} = \sum_{i=1}^3 \Delta \bar{\mathbf{t}}_i.$$

#### Consistency and asymptotic statistical efficiency test.

In our simulation, we run a total of  $K = 1000$  Monte Carlo tests to evaluate MSEs and biases. In order to verify our theoretical claim that the proposed CECME estimator is consistent and asymptotically statistically-efficient, we set  $m = 10, 30, 100, 300, 1000, 3000$  and evaluate the MSEs under varied noise intensities. The result is plotted in Fig. 3, where we use CECME1 and CECME2 to denote our first-step estimate and second-step estimate, respectively. We see that the MSE of the CECME1 estimate declines linearly w.r.t. the number of points in the log-log plot, which implies it is  $\sqrt{m}$ -consistent. In addition, with a one-step of GN iteration, the CECME2 estimate asymptotically reaches the CRB. Actually, when the point number exceeds one hundred, our estimator owns the statistical efficiency. It is noteworthy to see that our estimator outperforms the state-of-the-art ones, especially when the point number and noise intensity are relatively

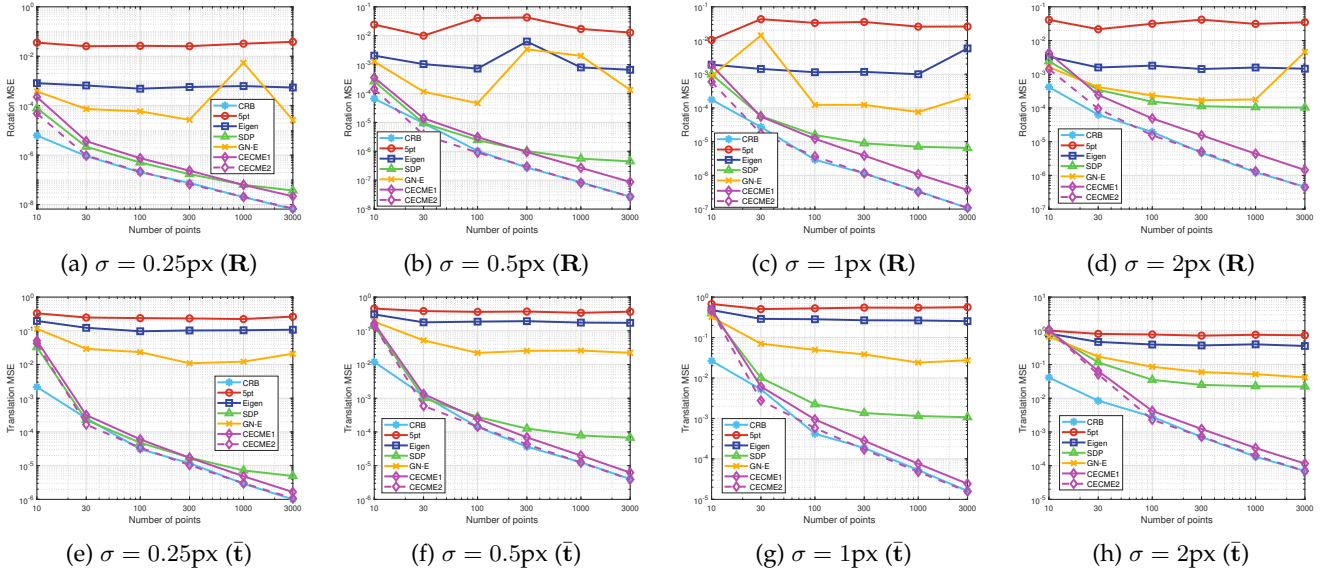


Figure 3: MSE comparison under different noise intensities and point numbers.

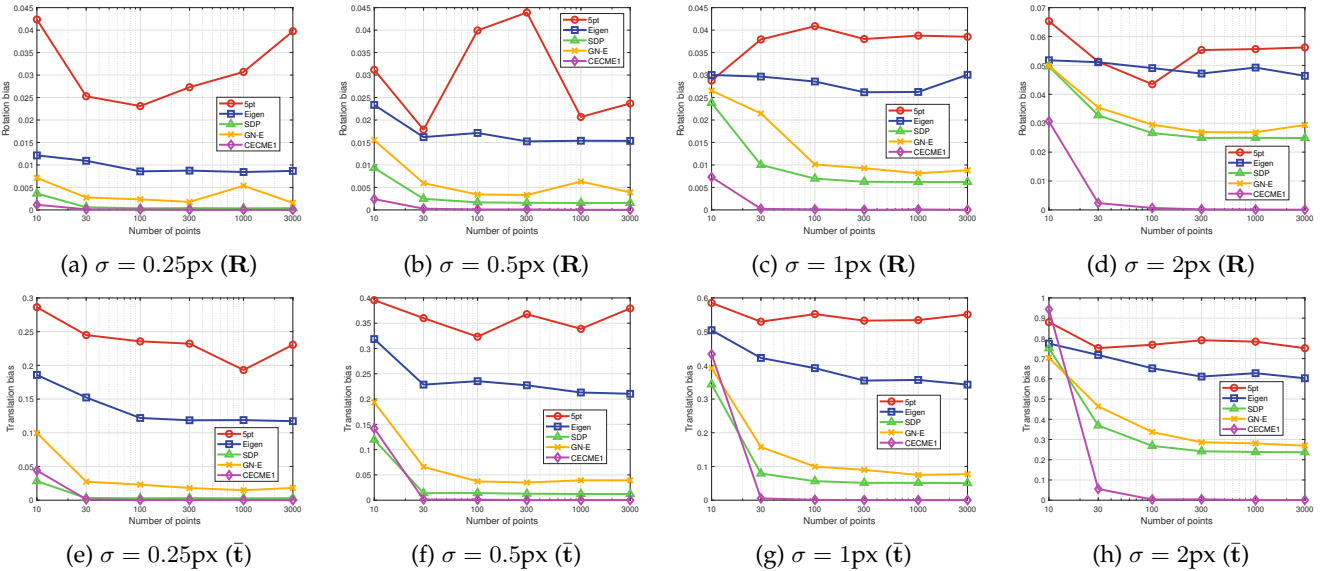


Figure 4: Bias comparison under different noise intensities and point numbers.

large. For the 5pt solver, since it only utilizes 5 point correspondences to infer relative pose, its MSE does not change w.r.t. the point number. A counter-intuitive phenomenon is that although Eigen and GN-E solvers use all  $m$  inputs in the pose inference, their MSEs do not vary obviously w.r.t.  $m$ , especially the Eigen solver. This is because their prior pose information is provided by the 5pt solver which has a constant estimation accuracy. It shows that Eigen and GN-E solvers highly depend on the quality of the initial estimate. For the SDP solver, it performs well in the case of small noise intensity. As the noise intensity increases, its performance deteriorates rapidly. This coincides with the theoretical development in [11], which says that only when the noise is small enough, the SDP relaxation is tight, and the SDP solver gives a global solution to problem (9).

We remark that the consistency of the CECME1 estimate

is owing to the proposed bias elimination (18) which leads to asymptotic unbiasedness. Asymptotic unbiasedness together with vanishing covariance finally yields consistency. The asymptotic unbiasedness of the CECME1 estimate is validated in Fig. 4, where we see that its bias converges to 0 as the point number increases. However, the bias of the other estimators cannot converge to 0, i.e., they are asymptotically biased. Actually, in the asymptotic case, their MSE is dominated by the asymptotic bias, and thus cannot converge to 0, as shown in Fig. 3.

**Influence of the length of translation.** In Assumption 1, we assume the true translation is not equal to 0, otherwise, the normalized translation cannot be identified, and the homography matrix should be estimated instead of the essential matrix. Nevertheless, it has been empirically shown that the length of translation  $\|t^o\|$  generally yields no impact

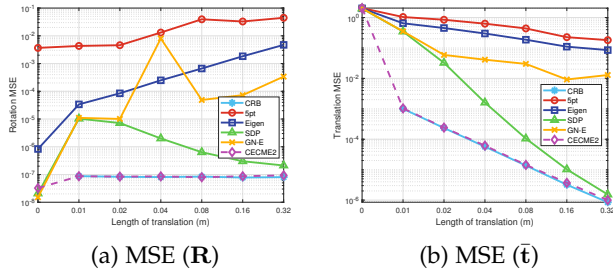


Figure 5: MSE under different lengths of translation.

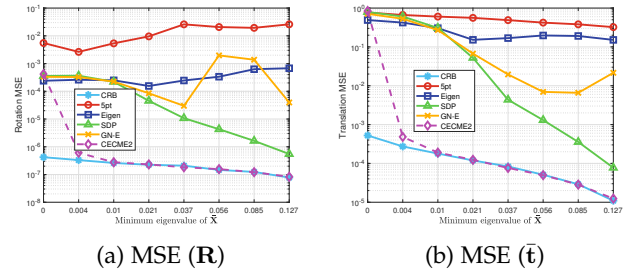


Figure 6: MSE under different point distributions.

on the estimation accuracy of the rotation matrix, even in the pure rotation cases, the rotation can be recovered from the essential matrix correctly [11]. In addition, there exists a statistic that can identify the pure rotation cases [38]. Specifically, the statistic is given as the average of  $\left\{ \frac{\mathbf{z}_i^h \times \tilde{\mathbf{R}} \mathbf{y}_i^h}{\|\mathbf{z}_i^h\| \|\mathbf{y}_i^h\|} \right\}_{i=1}^m$ , where  $\tilde{\mathbf{R}}$  is the estimate of the rotation matrix. This statistic can be utilized to appraise the estimation quality of the normalized translation.

In this experiment, we fix  $m = 1000$ ,  $\sigma = 0.5\text{px}$ , and change the length of the translation. The result is shown in Fig. 5. Note that when  $\|\mathbf{t}^o\| = 0$ , the Fisher information matrix is singular, and the CRB is not available. We see from the figure that the CRB of  $\mathbf{R}$  does not change w.r.t.  $\|\mathbf{t}^o\|$ , while the CRB of  $\bar{\mathbf{t}}$  increases as  $\|\mathbf{t}^o\|$  decreases. In addition, our estimator CECME2 coincides with the CRB for both  $\mathbf{R}$  and  $\bar{\mathbf{t}}$ . However, the other estimators have an obvious gap from the CRB, and their stability is not as good as ours. We also calculate the pure rotation statistics, and they are  $6.9e^{-4}$ ,  $2.6e^{-3}$ ,  $5.6e^{-3}$ ,  $1.1e^{-2}$ ,  $2.2e^{-2}$ ,  $4.5e^{-2}$ ,  $8.5e^{-2}$  respectively, which have the same varying trend as  $\|\mathbf{t}^o\|$ . Hence, it can serve as an indicator that depicts how confident we are with the estimation for  $\bar{\mathbf{t}}$ . The smaller the statistic is, the less accurate the estimate is.

**Influence of the distribution of 3D points.** In Assumption 2, we assume the 3D points  $\{\mathbf{x}_i\}_{i=1}^m$  and the two camera centers do not lie on a ruled quadric surface, which we call the degenerate configuration. The most likely degenerate configuration is that  $\{\mathbf{x}_i\}_{i=1}^m$  concentrate on a man-made plane, e.g., a wall. Similar to the case of  $\|\mathbf{t}^o\| = 0$ , in the coplanar case, the homography matrix should be estimated instead of the essential matrix. Let  $\tilde{\mathbf{X}} = [\mathbf{x}_1^h \ \dots \ \mathbf{x}_m^h][\mathbf{x}_1^h \ \dots \ \mathbf{x}_m^h]^T / m$ , where  $\mathbf{x}_i^h$  is the homogeneous coordinates of  $\mathbf{x}_i$ . Then, if  $\{\mathbf{x}_i\}_{i=1}^m$  are coplanar, it can be verified that  $\lambda_{\min}(\tilde{\mathbf{X}}) = 0$ . Therefore,  $\lambda_{\min}(\tilde{\mathbf{X}})$  is a quantity that can identify the coplanar case. In Fig. 6, we plot the relationship between MSE and  $\lambda_{\min}(\tilde{\mathbf{X}})$ . We see that as  $\lambda_{\min}(\tilde{\mathbf{X}})$  decreases, i.e., the 3D points shrink in some dimension, the CRB and MSE increase. However, different from the case of  $\|\mathbf{t}^o\| = 0$ , when  $\lambda_{\min}(\tilde{\mathbf{X}}) = 0$ , the Fisher information matrix is nonsingular and the CRB is available, which implies the relative pose is locally identifiable. Nevertheless, in the (near) coplanar case, the MSE of all estimators deviates from the CRB, showing that the relative pose is not globally identifiable. Note that  $\{\mathbf{x}_i\}_{i=1}^m$  are unavailable in practice, so we cannot obtain  $\lambda_{\min}(\tilde{\mathbf{X}})$ . In order to identify the coplanar case in real applications, one can estimate a homography matrix and treat the average residual as the

coplanar statistic [39]. The smaller the statistic is, the more possible the coplanar case is.

## 7.2 Experiment with real images

For the experiment with real images, we use the ETH3D dataset [22]. This dataset contains 25 scenarios ranging from indoors to outdoors. In each scenario, there are consecutive images taken at different poses. The intrinsic and extrinsic parameters of the camera are given, so we can calculate the normalized image coordinates of each feature point and the true relative pose between an image pair. In addition, the 3D global map is available, and the 2D-3D point correspondences are provided, based on which the 2D-2D point correspondences can be obtained.

All algorithms are implemented in C++ via a PC equipped with an Intel Core i5-10400H and a 32Gb RAM. The evaluation details and codes are open source at [https://github.com/LIAS-CUHKSZ/epipolar\\_eval](https://github.com/LIAS-CUHKSZ/epipolar_eval). To validate that the proposed estimator has advantages in the asymptotic case, we only estimate the relative pose of an image pair (the two images are not necessarily consecutive) that has more than 200 point correspondences. The estimation errors of the rotation matrix and normalized translation vector are given by Frobenius norm and  $\ell_2$ -norm, respectively. Different from the simulation, since there may be outliers in real datasets, we first implement a rough RANSAC algorithm to clean the data. In addition, we run a refined RANSAC algorithm to provide the prior relative pose for Eigen and GN-E solvers. The minimal solver in both RANSAC algorithms is the 5pt estimator.

The accumulated estimation errors in all 25 scenarios are listed in Table 1, where “5pt” represents the result of the refined RANSAC algorithm based on the 5pt solver. We see that our proposed estimator CECME performs best in 18 scenarios for  $\mathbf{R}$  and 19 scenarios for  $\bar{\mathbf{t}}$ . It is noteworthy to see that Eigen and GN-E outperform SDP and sometimes become the best ones, which does not coincide with the simulation result. This is because, in real image tests, the 5pt solver is embedded in RANSAC algorithms and can provide more accurate prior information for Eigen and GN-E solvers. The average CPU time cost is listed in Table 2. Since Eigen and GN-E solvers need prior relative pose, their CPU time includes that of the 5pt method. We see that our CECME estimator consumes the least time and is suitable for real-time implementation in real applications — in the relief scenario which has the most average point number, it outputs the estimation result in a frequency near 100Hz.

Table 1: Accumulated estimation errors in all 25 scenarios. The quantity inside each bracket denotes the average point number of the associated scenario.

Scenario	5pt		Eigen		SDP		GN-E		CECME	
	R	$\bar{t}$	R	$\bar{t}$	R	$\bar{t}$	R	$\bar{t}$	R	$\bar{t}$
relief (1581)	0.8061	1.0508	0.2587	0.3798	0.3159	0.7732	0.2454	0.3862	<b>0.2093</b>	<b>0.3395</b>
door (1493)	0.0396	0.1027	0.0123	0.0411	0.0166	0.0619	0.0107	0.0340	<b>0.0106</b>	<b>0.0339</b>
observatory (1233)	1.1626	3.299	0.5861	1.8611	0.6498	2.1177	0.5911	1.8305	<b>0.5656</b>	<b>1.7956</b>
facade (1137)	4.3153	8.5206	<b>1.6686</b>	<b>3.9798</b>	3.0156	13.8916	1.7408	4.0198	1.6697	4.7817
boulders (1063)	0.5356	1.0433	0.1523	0.3229	0.1919	0.3350	<b>0.1419</b>	0.3147	0.1438	<b>0.3014</b>
courtyard (1044)	15.564	11.870	11.416	8.5707	13.791	15.849	12.065	8.4889	<b>6.6839</b>	<b>5.8835</b>
relief 2 (935)	0.4077	0.7491	<b>0.1356</b>	0.2505	0.1707	0.3602	0.1443	0.2615	0.1373	<b>0.2284</b>
statue (872)	0.0621	0.0409	0.0196	<b>0.0133</b>	0.0217	0.0150	0.0194	0.0141	<b>0.0187</b>	0.0135
bridge (846)	1.5694	2.3619	0.7380	3.0056	0.8237	1.0468	0.7578	1.0497	<b>0.6751</b>	<b>0.9231</b>
terrace 2 (809)	0.1140	0.4017	0.0535	0.1526	0.0554	0.1782	0.0543	0.1528	<b>0.0466</b>	<b>0.1267</b>
delivery area (780)	0.9413	1.5425	0.3083	0.6972	0.7291	2.6973	0.2857	0.6297	<b>0.2557</b>	<b>0.4688</b>
exhibition hall (708)	4.9612	21.618	2.7149	16.206	5.5919	46.645	5.2199	14.558	<b>1.8387</b>	<b>13.087</b>
electro (687)	0.5948	1.5209	0.2086	0.4493	0.2683	0.5138	0.2046	0.4369	<b>0.1893</b>	<b>0.3888</b>
terrace (629)	0.2766	0.4484	0.1098	0.1680	0.1277	0.1861	0.1117	0.1694	<b>0.1045</b>	<b>0.1538</b>
kicker (607)	1.2514	1.7623	0.4802	0.9699	0.6684	2.4542	0.4307	0.8965	<b>0.4148</b>	<b>0.5781</b>
botanical garden (602)	0.1468	0.5657	0.0711	0.2489	0.1016	0.2753	0.0743	0.2580	<b>0.0602</b>	<b>0.1939</b>
terrains (569)	0.8063	0.9382	0.2669	0.2883	0.3854	0.7529	<b>0.2360</b>	<b>0.2691</b>	0.2698	0.3697
living room (505)	1.0608	2.6071	0.3765	<b>1.0791</b>	0.4231	1.2172	0.3739	1.0843	<b>0.3631</b>	1.1067
playground (498)	0.3226	0.6020	0.1225	0.2593	0.1452	0.2807	0.1241	0.2608	<b>0.1128</b>	<b>0.2312</b>
pipes (444)	0.0550	0.1098	0.0187	0.0214	0.0206	0.0553	<b>0.0166</b>	0.0174	0.0169	<b>0.0171</b>
lecture room (400)	0.3646	0.9807	0.0768	<b>0.1514</b>	0.0849	0.1601	0.0859	0.1583	<b>0.0758</b>	0.1584
lounge (349)	0.1176	0.3229	0.0512	0.1244	0.0529	0.1262	0.0501	0.1218	<b>0.0299</b>	<b>0.0759</b>
meadow (307)	0.0630	0.1275	0.0335	0.0602	0.0465	0.1043	<b>0.0319</b>	<b>0.0576</b>	0.0383	0.0639
office (294)	0.2995	1.6401	<b>0.2434</b>	1.5664	0.4674	2.7684	0.2435	1.5560	0.3067	<b>1.3621</b>
old computer (276)	0.2847	1.4734	0.1394	0.7114	0.1601	0.9491	0.1375	0.7362	<b>0.1125</b>	<b>0.5371</b>

Table 2: Average CPU time (unit:  $\mu s$ ) comparison in all 25 scenarios

Scenario	5pt	Eigen	SDP	GN-E	CECME						
relief	23650.1	23806.2	16721.1	44666.6	<b>11173.4</b>	electro	34637.8	34781.6	11371.7	43759.1	<b>4769.1</b>
door	19416.8	19569.5	16487.5	39572.4	<b>10822.9</b>	terrace	32920.6	33063.8	11050.0	41492.2	<b>4543.6</b>
observatory	26349.6	26497.3	14718.3	43162.2	<b>8908.4</b>	kicker	26675.1	26827.5	10803.1	34901.4	<b>4439.3</b>
facade	18865.6	19001.0	12734.5	31995.4	<b>7124.1</b>	botanical garden	33201.3	33339.3	10096.3	41267.3	<b>4368.7</b>
boulders	21263.6	21424.5	13706.4	35533.4	<b>7424.5</b>	terrains	16304.9	16437.6	8873.2	22665.2	<b>3390.4</b>
courtyard	13562.2	13752.6	13847.4	27610.4	<b>7459.6</b>	living room	15296.7	15445.7	10206.9	22167.7	<b>3829.1</b>
relief 2	18950.4	19087.7	12770.0	31956.1	<b>6770.6</b>	playground	27478.8	27612.2	9848.0	34254.6	<b>3692.3</b>
statue	22514.8	22652.6	12224.1	34187.9	<b>6269.4</b>	pipes	14474.1	14621.1	9904.0	20505.7	<b>3401.6</b>
bridge	30885.1	31023.0	11686.7	41528.3	<b>5681.5</b>	lecture room	14437.3	14568.5	10184.7	19739.8	<b>2859.1</b>
terrace 2	17060.3	17202.0	12211.5	28127.5	<b>5883.5</b>	lounge	29295.0	29442.6	8908.1	35007.8	<b>2655.4</b>
delivery area	23891.9	24038.9	11819.0	34348.4	<b>5541.0</b>	meadow	15526.6	15690.8	9117.3	19973.1	<b>2606.4</b>
exhibition hall	14373.2	14527.2	11506.7	23975.9	<b>5130.2</b>	office	22076.7	22224.3	8812.1	26172.8	<b>2256.4</b>
						old computer	18101.6	18239.2	8552.9	21944.2	<b>2081.5</b>

We select four scenarios where our estimator has the smallest accumulated estimation errors and plot the error distribution in Fig. 7. We find that the reasons why the proposed CECME solver performs best fall into two folds: In relief, old computer, and lounge scenarios, it is mainly because CECME produces less severe outlier estimates; While in the botanical garden scenario, it is mainly because CECME has lower quartiles.

To test the relationship between the MSE and point number, we randomly select four image pairs that have abun-

dant point correspondences. For each pair, we randomly select a certain number of points to infer the camera motion, and the MSE is calculated by 100 Monte Carlo trials. The result is plotted in Fig. 8. We see that the MSE of our CECME solver consistently declines as the point number increases. Moreover, it outperforms the other solvers when the point number reaches the order of hundreds, which indicates the bias elimination and GN iteration on  $SO(3)$  and 2-sphere embedded in our algorithm do play a role.

We also test the CPU time of all algorithms under dif-

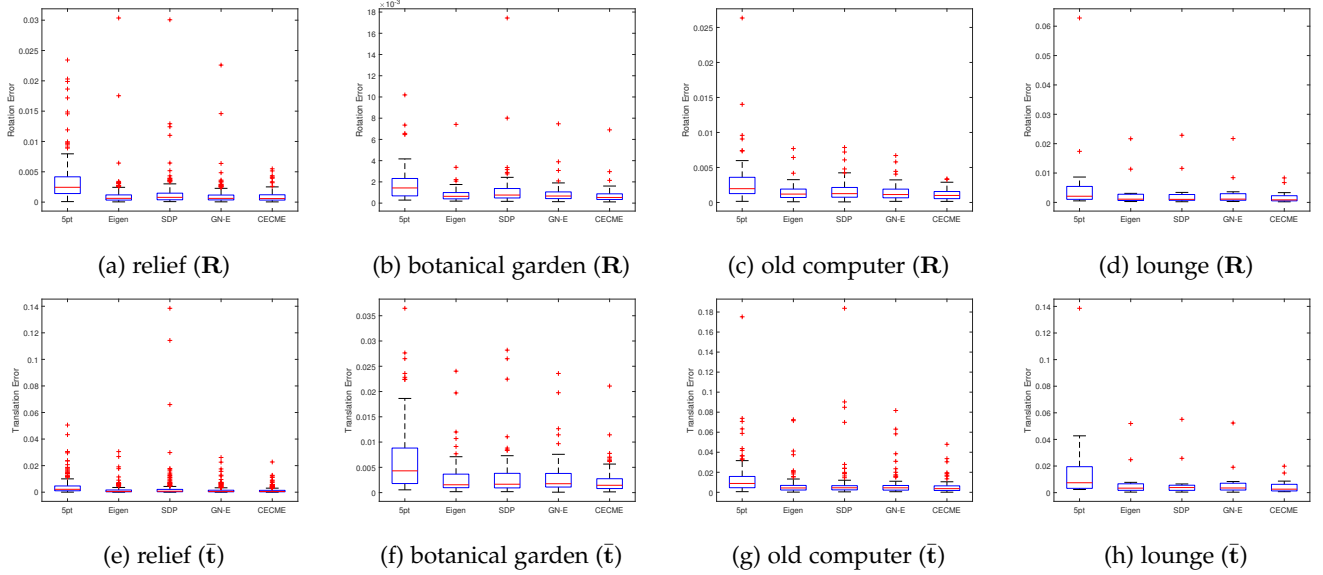


Figure 7: Error distribution of the scenarios of relief, botanical garden, old computer, and lounge.

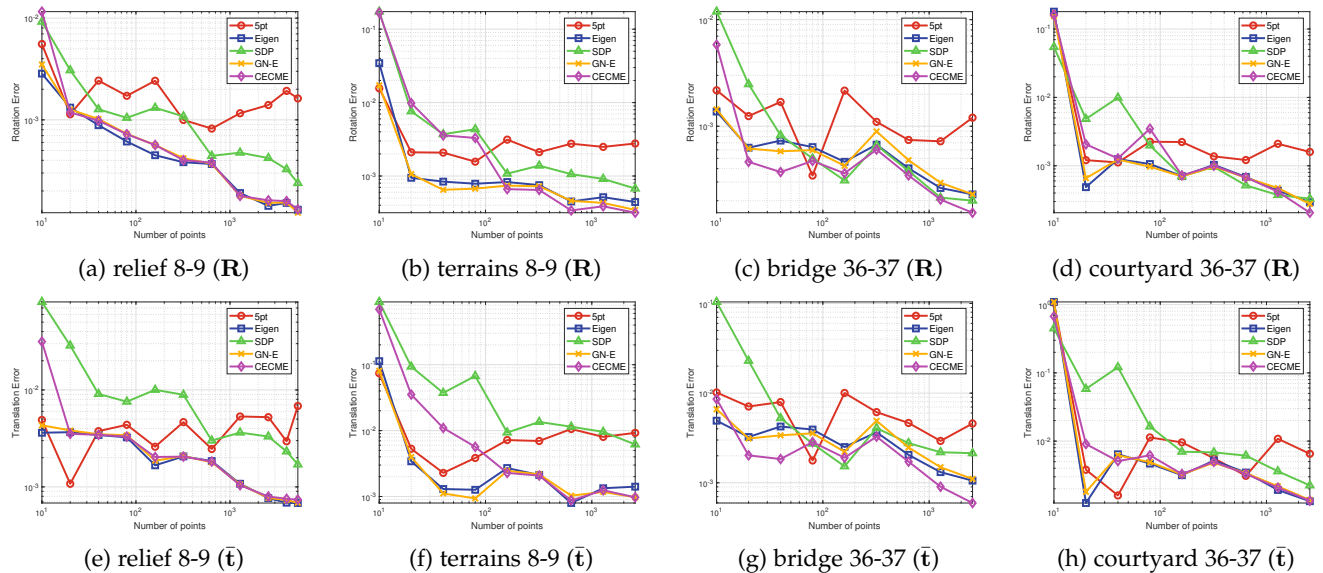


Figure 8: Consistency test of four image pairs with abundant point correspondences. “relief 8-9” means the image pair consists of the eighth and ninth images in the relief scenario.

ferent numbers of points. The image pair used is “facade 8-9”, where the number of point correspondences is 4357. We perform 100 Monte Carlo trials to evaluate the average CPU time for each point number. The result is shown in Fig. 10. Our proposed algorithm has the least CPU time constantly, and when  $m = 2560$ , its average CPU time is 14ms, showing the capacity of real-time implementation. We see that the Eigen solver costs almost the same time as the 5pt one. This is partially because it uses the rotation estimate of the 5pt solver as the prior information and does not need to conduct the **recoverPose** function to recover the relative pose from the essential matrix, which involves triangulating all 3D points using the SVD. It only needs to judge the binary sign of  $\bar{\mathbf{t}}$  by testing the angle between  $\bar{\mathbf{t}}$  and the vector connecting each point correspondence. In

addition, we note that when the point number is relatively small, the SDP solver costs the most time, while as the point number increases, the GN-E solver becomes the most time-consuming one.

Finally, we present in Fig. 9 some typical degenerate scenarios where our algorithm yields a relatively large estimation error. In Fig. 9(a), the points concentrate on the roof of the office, which violates the noncoplanar Assumption 2; In Fig. 9(b), the translation between the image pair is too small, which can be viewed as the pure rotation case and infringes Assumption 1; In Fig. 9(c), the 3D points are confined within a very limited range in two dimensions and has a small  $\lambda_{\min}(\bar{\mathbf{X}})$ ; In Fig. 9(d), most of the 3D points locate on leaves, whose position may change due to the disturbance of wind and in turn weaken the estimation

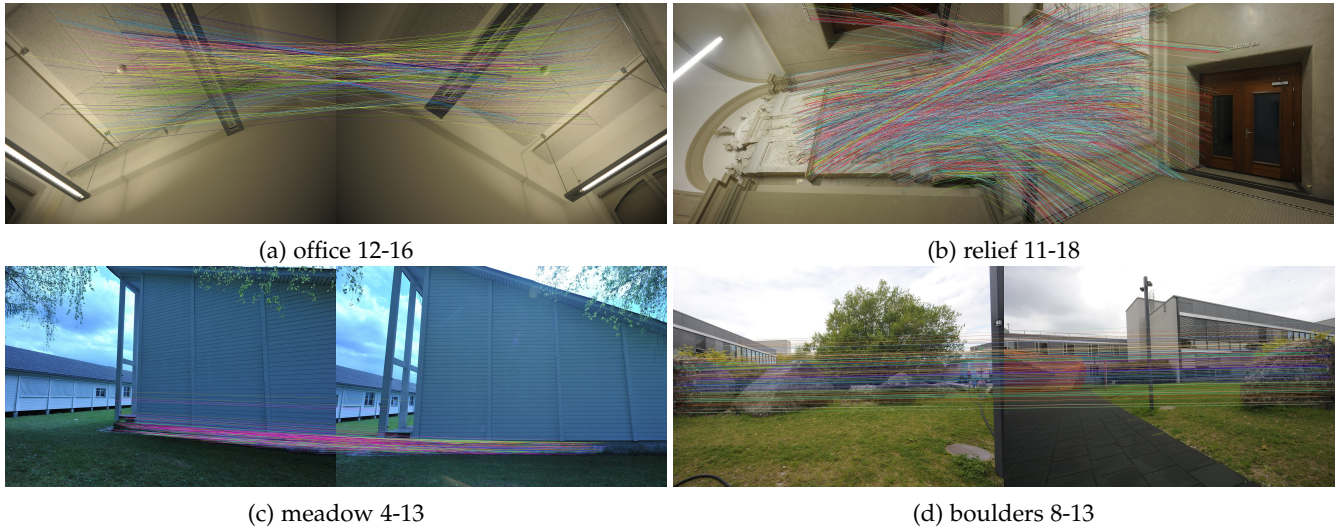


Figure 9: Some examples of degenerate scenarios.

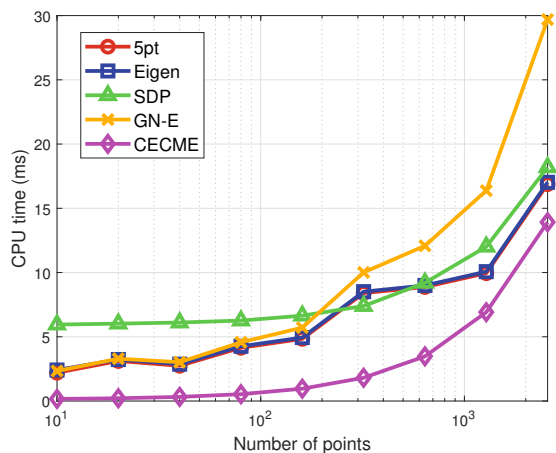


Figure 10: CPU time comparison under different point numbers.

accuracy. The above degenerate scenarios pose a challenge to the monocular-vision-based relative pose estimation. To overcome this issue, more sensor information, e.g., binocular camera and IMU, could be incorporated into odometry and SLAM systems [40], [41].

## 8 CONCLUSION

In this paper, we have revisited the CME problem that plays an important role in many computer vision applications. We derived the original measurement model associated with the rotation matrix and normalized translation, based on which the ML problem was formulated. To optimally solve the ML problem in the asymptotic case, we first estimated the noise variance by calculating the maximum eigenvalue of a  $9 \times 9$  matrix. Based on the  $\sqrt{m}$ -consistent noise variance estimate, we then proposed a two-step estimator that has the same asymptotic statistical property as the ML estimator, i.e., consistency and asymptotic efficiency. We showed that our algorithm has  $O(m)$  time complexity. Experiments

on both synthetic data and real images demonstrated that when the point number reaches the order of hundreds, the proposed algorithm outperforms the state-of-the-art ones in terms of MSE and CPU time. It is noteworthy to see that the value of  $\|t\|$  hardly affects the estimation of the rotation matrix, but has a significant effect on the translation. In addition, there exists a pure rotation statistic that can efficiently evaluate the estimation quality of the translation. Hence, the assumption that  $\|t\| \neq 0$  can be relaxed in real applications. We also presented some typical degenerate scenarios where our algorithm may not be stable.

## APPENDIX A PROOF OF THEOREM 1

The proof is mainly based on the following lemma:

**Lemma 2** ([42, Lemma 6]). *Let  $\mathbf{R}$  and  $\mathbf{S}$  be two real symmetric matrices and  $\mathbf{Q} = \mathbf{R} + \mathbf{S}$ . If  $\mathbf{Q}$  is positive-definite and  $\mathbf{R}$  is positive-semidefinite with 0 eigenvalues, then  $\lambda_{\max}(\mathbf{Q}^{-1}\mathbf{S}) = 1$ .*

First, we show the positive definiteness of  $\mathbf{Q}_m$  when  $m \geq 9$ . Note that

$$\text{rank}(\mathbf{A}_m) = \text{rank} \begin{pmatrix} \mathbf{z}_1^{h\top} \mathbf{L}_1 \\ \vdots \\ \mathbf{z}_m^{h\top} \mathbf{L}_m \end{pmatrix} = \text{rank} \begin{pmatrix} \mathbf{z}_1^{h\top} \otimes \mathbf{y}_1^{h\top} \\ \vdots \\ \mathbf{z}_m^{h\top} \otimes \mathbf{y}_m^{h\top} \end{pmatrix}.$$

Given Assumption 2,  $\mathbf{y}_i, i = 1, \dots, m$  are not collinear. Hence, the column rank of the matrix  $[\mathbf{y}_1^h \dots \mathbf{y}_m^h]^\top$  is 3. By further combining the fact that  $\mathbf{z}_i, i \in \{1, \dots, m\}$  are independent random variables, it holds that the matrix  $\mathbf{A}_m$  has full column rank with probability one. Since  $\mathbf{Q}_m$  has the same rank as  $\mathbf{A}_m$ , we have that  $\mathbf{Q}_m$  is positive-definite with probability one. Next, we construct a positive-semidefinite matrix with 0 eigenvalues. Let  $\mathbf{A}_m^o$  be the noise-free counterpart of  $\mathbf{A}_m$ , i.e.,  $\mathbf{A}_m^o = [\mathbf{L}_1^\top \mathbf{z}_1^{ho} \dots \mathbf{L}_m^\top \mathbf{z}_m^{ho}]^\top$ , where  $\mathbf{z}_i^{ho}$  is the noise-free counterpart of  $\mathbf{z}_i^h$ . Since  $\mathbf{z}_i^{ho\top} \mathbf{E} \mathbf{y}_i^h = 0$  (epipolar geometry), we have  $\mathbf{A}_m^o \boldsymbol{\theta} = \mathbf{0}$ . Given Assumption 1,  $\boldsymbol{\theta} = \text{vec}(\mathbf{E}) \neq \mathbf{0}$ , which implies that the matrix  $\mathbf{A}_m^o$  is not full column rank, and  $\boldsymbol{\theta}$  is an eigenvector of  $\mathbf{A}_m^o$

associated with the 0 eigenvalue. Let  $\mathbf{Q}_m^o = \mathbf{A}_m^{o\top} \mathbf{A}_m^o / m$ . Then the matrix  $\mathbf{Q}_m^o$  is positive-semidefinite with at least one 0 eigenvalue. The following lemma plays an important role in identifying the relationship among  $\mathbf{Q}_m$ ,  $\mathbf{Q}_m^o$ , and  $\mathbf{S}_m$ :

**Lemma 3** ([43, Lemma 4]). *Let  $\{X_i\}$  be a sequence of independent random variables with  $\mathbb{E}[X_i] = 0$  and  $\mathbb{E}[X_i^2] \leq \varphi < \infty$  for all  $i$ . Then, there holds  $\sum_{i=1}^m X_i / m = O_p(1/\sqrt{m})$ .*

Based on Lemma 3, it can be verified that

$$\mathbf{Q}_m = \mathbf{Q}_m^o + \sigma^2 \mathbf{S}_m + O_p(1/\sqrt{m}). \quad (26)$$

Further, note that  $\mathbf{Q}_m$  is positive-definite,  $\mathbf{Q}_m^o$  is positive-semidefinite with 0 eigenvalues, and  $O_p(1/\sqrt{m})$  is a quantity that converges to 0 at a rate of  $1/\sqrt{m}$ . According to Lemma 2, it holds that  $\lambda_{\max}(\mathbf{Q}_m^{-1} \sigma^2 \mathbf{S}_m)$  converges to 1 at a rate of  $1/\sqrt{m}$ . In other words,  $\hat{\sigma}_m^2 = 1/\lambda_{\max}(\mathbf{Q}_m^{-1} \mathbf{S}_m)$  converges to  $\sigma^2$  at a rate of  $1/\sqrt{m}$ , which completes the proof.

## APPENDIX B DERIVATION OF GN ITERATIONS ON SO(3) AND 2-SPHERE

The measurement equation (6) can be rephrased as

$$\mathbf{z}_i = \frac{\mathbf{W}(\mathbf{L}_i \text{vec}(\mathbf{R}) + k_i \bar{\mathbf{t}})}{\mathbf{e}_3^\top (\mathbf{L}_i \text{vec}(\mathbf{R}) + k_i \bar{\mathbf{t}})} + \boldsymbol{\epsilon}_i. \quad (27)$$

Define

$$\begin{aligned} \mathbf{g}_i(\mathbf{s}, \alpha, \beta) &= \mathbf{W}(\mathbf{L}_i \text{vec}(\hat{\mathbf{R}}_m^{\text{BE}} \exp(\mathbf{s}^\wedge)) + k_i(\mathbf{s}, \alpha, \beta) \bar{\mathbf{t}}(\alpha, \beta)), \\ h_i(\mathbf{s}, \alpha, \beta) &= \mathbf{e}_3^\top (\mathbf{L}_i \text{vec}(\hat{\mathbf{R}}_m^{\text{BE}} \exp(\mathbf{s}^\wedge)) + k_i(\mathbf{s}, \alpha, \beta) \bar{\mathbf{t}}(\alpha, \beta)), \\ \mathbf{u}_i(\mathbf{s}, \alpha, \beta) &= \frac{\mathbf{W}(\mathbf{L}_i \text{vec}(\hat{\mathbf{R}}_m^{\text{BE}} \exp(\mathbf{s}^\wedge)) + k_i(\mathbf{s}, \alpha, \beta) \bar{\mathbf{t}}(\alpha, \beta))}{\mathbf{e}_3^\top (\mathbf{L}_i \text{vec}(\hat{\mathbf{R}}_m^{\text{BE}} \exp(\mathbf{s}^\wedge)) + k_i(\mathbf{s}, \alpha, \beta) \bar{\mathbf{t}}(\alpha, \beta))}, \end{aligned}$$

where  $k_i(\mathbf{s}, \alpha, \beta)$  is defined by substituting  $\mathbf{R}$  with  $\hat{\mathbf{R}}_m^{\text{BE}} \exp(\mathbf{s}^\wedge)$  and  $\bar{\mathbf{t}}$  with  $\bar{\mathbf{t}}(\alpha, \beta)$  in (22). Then we have

$$\begin{aligned} \frac{\partial \mathbf{u}_i}{\partial \mathbf{s}^\top} &= \frac{(h_i(\mathbf{0}) \mathbf{W} - \mathbf{g}_i(\mathbf{0}) \mathbf{e}_3^\top) (\boldsymbol{\Psi}_i + \bar{\mathbf{t}}(\mathbf{0}) \partial k_i / \partial \mathbf{s}^\top)}{h_i(\mathbf{0})^2}, \\ \frac{\partial \mathbf{u}_i}{\partial \alpha} &= \frac{(h_i(\mathbf{0}) \mathbf{W} - \mathbf{g}_i(\mathbf{0}) \mathbf{e}_3^\top) (k_i \boldsymbol{\Phi} + \bar{\mathbf{t}}(\mathbf{0}) \partial k_i / \partial \alpha)}{h_i(\mathbf{0})^2}, \\ \frac{\partial \mathbf{u}_i}{\partial \beta} &= \frac{(h_i(\mathbf{0}) \mathbf{W} - \mathbf{g}_i(\mathbf{0}) \mathbf{e}_3^\top) (k_i \boldsymbol{\Theta} + \bar{\mathbf{t}}(\mathbf{0}) \partial k_i / \partial \beta)}{h_i(\mathbf{0})^2}, \end{aligned}$$

where all partial derivatives are evaluated at  $\mathbf{s}, \alpha, \beta = 0$ , and

$$\begin{aligned} \boldsymbol{\Psi}_i &= \mathbf{y}_i^{h\top} \otimes \hat{\mathbf{R}}_m^{\text{BE}} \frac{\partial \text{vec}(\exp(\mathbf{s}^\wedge))}{\partial \mathbf{s}^\top}, \\ \boldsymbol{\Phi} &= \frac{\partial \bar{\mathbf{t}}(\alpha, \beta)}{\partial \alpha} = \begin{bmatrix} -\sin \alpha_0 \cos \beta_0 \\ -\sin \alpha_0 \sin \beta_0 \\ \cos \alpha_0 \end{bmatrix}, \\ \boldsymbol{\Theta} &= \frac{\partial \bar{\mathbf{t}}(\alpha, \beta)}{\partial \beta} = \begin{bmatrix} -\cos \alpha_0 \sin \beta_0 \\ \cos \alpha_0 \cos \beta_0 \\ 0 \end{bmatrix}, \end{aligned}$$

and  $\partial k_i / \partial \mathbf{s}^\top$ ,  $\partial k_i / \partial \alpha$ ,  $\partial k_i / \partial \beta$  are given in (24), where den and num represent the denominator and numerator of  $k_i$  in (22), respectively.

Then we can obtain the Jacobian matrix

$$\mathbf{J} = \begin{bmatrix} \vdots & \vdots & \vdots \\ \frac{\partial \mathbf{u}_i}{\partial \mathbf{s}^\top} & \frac{\partial \mathbf{u}_i}{\partial \alpha} & \frac{\partial \mathbf{u}_i}{\partial \beta} \\ \vdots & \vdots & \vdots \end{bmatrix} \in \mathbb{R}^{2m \times 5}.$$

The GN iteration is

$$\begin{bmatrix} \hat{\mathbf{s}}_m^{\text{GN}} \\ \hat{\alpha}_m^{\text{GN}} \\ \hat{\beta}_m^{\text{GN}} \end{bmatrix} = \begin{bmatrix} \mathbf{0} \\ \alpha_0 \\ \beta_0 \end{bmatrix} + (\mathbf{J}^\top \mathbf{J})^{-1} \mathbf{J}^\top \mathbf{r}, \quad (28)$$

where  $\mathbf{r} = [\mathbf{r}_1^\top \cdots \mathbf{r}_m^\top]^\top$ .

$$\begin{aligned} \frac{\partial k_i}{\partial \mathbf{s}^\top} &= \frac{\text{den}(\mathbf{y}_i^{h\top} \hat{\mathbf{R}}_m^{\text{BE}\top} (\mathbf{C}_1 \mathbf{I}_3 \otimes \bar{\mathbf{t}} + \mathbf{I}_3 \otimes \bar{\mathbf{t}}^\top \mathbf{C}_1^\top) \boldsymbol{\Psi}_i) - \text{num}(\bar{\mathbf{t}}^\top \mathbf{C}_2 \mathbf{I}_3 \otimes \bar{\mathbf{t}} \boldsymbol{\Psi}_i)}{\text{den}^2}, \\ \frac{\partial k_i}{\partial \alpha} &= \frac{\text{den}(\mathbf{y}_i^{h\top} \hat{\mathbf{R}}_m^{\text{BE}\top} \mathbf{C}_1 (\hat{\mathbf{R}}_m^{\text{BE}} \mathbf{y}_i^h) \otimes \mathbf{I}_3 \boldsymbol{\Phi}) - \text{num}(\bar{\mathbf{t}}^\top \mathbf{C}_2 (\hat{\mathbf{R}}_m^{\text{BE}} \mathbf{y}_i^h) \otimes \mathbf{I}_3 + (\hat{\mathbf{R}}_m^{\text{BE}} \mathbf{y}_i^h)^\top \otimes \bar{\mathbf{t}}^\top \mathbf{C}_2^\top) \boldsymbol{\Phi}}{\text{den}^2}, \\ \frac{\partial k_i}{\partial \beta} &= \frac{\text{den}(\mathbf{y}_i^{h\top} \hat{\mathbf{R}}_m^{\text{BE}\top} \mathbf{C}_1 (\hat{\mathbf{R}}_m^{\text{BE}} \mathbf{y}_i^h) \otimes \mathbf{I}_3 \boldsymbol{\Theta}) - \text{num}(\bar{\mathbf{t}}^\top \mathbf{C}_2 (\hat{\mathbf{R}}_m^{\text{BE}} \mathbf{y}_i^h) \otimes \mathbf{I}_3 + (\hat{\mathbf{R}}_m^{\text{BE}} \mathbf{y}_i^h)^\top \otimes \bar{\mathbf{t}}^\top \mathbf{C}_2^\top) \boldsymbol{\Theta}}{\text{den}^2}. \end{aligned} \quad (24)$$

$$\begin{aligned} \frac{\partial k_i}{\partial \boldsymbol{\xi}_R^\top} &= \frac{\text{den}(\mathbf{y}_i^{h\top} \hat{\mathbf{R}}_m^{\text{BE}\top} (\mathbf{C}_1 \mathbf{I}_3 \otimes \bar{\mathbf{t}} + \mathbf{I}_3 \otimes \bar{\mathbf{t}}^\top \mathbf{C}_1^\top) \mathbf{L}_i) - \text{num}(\bar{\mathbf{t}}^\top \mathbf{C}_2 \mathbf{I}_3 \otimes \bar{\mathbf{t}} \mathbf{L}_i)}{\text{den}^2}, \\ \frac{\partial k_i}{\partial \bar{\mathbf{t}}^\top} &= \frac{\text{den}(\mathbf{y}_i^{h\top} \hat{\mathbf{R}}_m^{\text{BE}\top} \mathbf{C}_1 (\hat{\mathbf{R}}_m^{\text{BE}} \mathbf{y}_i^h) \otimes \mathbf{I}_3) - \text{num}(\bar{\mathbf{t}}^\top \mathbf{C}_2 (\hat{\mathbf{R}}_m^{\text{BE}} \mathbf{y}_i^h) \otimes \mathbf{I}_3 + (\hat{\mathbf{R}}_m^{\text{BE}} \mathbf{y}_i^h)^\top \otimes \bar{\mathbf{t}}^\top \mathbf{C}_2^\top)}{\text{den}^2}. \end{aligned} \quad (25)$$

## APPENDIX C

### PROOF OF THEOREM 3

Let  $f_m(\mathbf{s}, \alpha, \beta)$  denote the objective function of (8), where  $\mathbf{R} = \hat{\mathbf{R}}_m^{\text{BE}} \exp(\mathbf{s}^\wedge)$  and  $\bar{\mathbf{t}} = \bar{\mathbf{t}}(\alpha, \beta)$ , and denote the optimal  $\mathbf{s}$ ,  $\alpha$ , and  $\beta$  as  $\hat{\mathbf{s}}_m^{\text{ML}}$ ,  $\hat{\alpha}_m^{\text{ML}}$ , and  $\hat{\beta}_m^{\text{ML}}$ . Since  $\hat{\mathbf{R}}_m^{\text{BE}}$  and  $\hat{\mathbf{t}}_m^{\text{BE}}$  are  $\sqrt{m}$ -consistent, it holds that

$$\begin{bmatrix} \hat{\mathbf{s}}_m^{\text{ML}} \\ \hat{\alpha}_m^{\text{ML}} \\ \hat{\beta}_m^{\text{ML}} \end{bmatrix} - \begin{bmatrix} \mathbf{0} \\ \alpha_0 \\ \beta_0 \end{bmatrix} = O_p(1/\sqrt{m}).$$

Based on the optimality condition  $\nabla f_m(\hat{\mathbf{s}}_m^{\text{ML}}, \hat{\alpha}_m^{\text{ML}}, \hat{\beta}_m^{\text{ML}}) = \mathbf{0}$  and the Taylor expansion, we have

$$\mathbf{0} = \nabla f_{m,0} + \nabla^2 f_{m,0} \begin{bmatrix} \hat{\mathbf{s}}_m^{\text{ML}} - \mathbf{0} \\ \hat{\alpha}_m^{\text{ML}} - \alpha_0 \\ \hat{\beta}_m^{\text{ML}} - \beta_0 \end{bmatrix} + o_p\left(\frac{1}{\sqrt{m}}\right),$$

where we use  $f_{m,0}$  for the abbreviation of  $f_m(\mathbf{0}, \alpha_0, \beta_0)$ . Then,

$$\begin{bmatrix} \hat{\mathbf{s}}_m^{\text{ML}} - \mathbf{0} \\ \hat{\alpha}_m^{\text{ML}} - \alpha_0 \\ \hat{\beta}_m^{\text{ML}} - \beta_0 \end{bmatrix} = -\nabla^2 f_{m,0}^{-1} \nabla f_{m,0} + o_p\left(\frac{1}{\sqrt{m}}\right).$$

By combining the GN iteration (28), we finally obtain

$$\begin{aligned} & \begin{bmatrix} \hat{\mathbf{s}}_m^{\text{ML}} - \hat{\mathbf{s}}_m^{\text{GN}} \\ \hat{\alpha}_m^{\text{ML}} - \hat{\alpha}_m^{\text{GN}} \\ \hat{\beta}_m^{\text{ML}} - \hat{\beta}_m^{\text{GN}} \end{bmatrix} \\ &= -\nabla^2 f_{m,0}^{-1} \nabla f_{m,0} - (\mathbf{J}^\top \mathbf{J})^{-1} \mathbf{J}^\top \mathbf{r} + o_p\left(\frac{1}{\sqrt{m}}\right) \\ &= \left( \frac{2\nabla^2 f_{m,0}^{-1}}{m} - \frac{(\mathbf{J}^\top \mathbf{J})^{-1}}{m} \right) \mathbf{J}^\top \mathbf{r} + o_p\left(\frac{1}{\sqrt{m}}\right) \\ &= O_p\left(\frac{1}{\sqrt{m}}\right) O_p\left(\frac{1}{\sqrt{m}}\right) + o_p\left(\frac{1}{\sqrt{m}}\right) \\ &= o_p\left(\frac{1}{\sqrt{m}}\right), \end{aligned}$$

where the third “=” is based on Lemma 3 in Appendix A. Since the exp, sin, cos are all continuous functions, we have  $\hat{\mathbf{R}}_m^{\text{ML}} - \hat{\mathbf{R}}_m^{\text{GN}} = o_p(1/\sqrt{m})$  and  $\hat{\mathbf{t}}_m^{\text{ML}} - \hat{\mathbf{t}}_m^{\text{GN}} = o_p(1/\sqrt{m})$ , which completes the proof.

## APPENDIX D

### THE CRAMER-RAO BOUND

Define

$$\begin{aligned} \mathbf{g}'_i(\mathbf{R}, \bar{\mathbf{t}}) &= \mathbf{W}(\mathbf{R}\mathbf{y}_i^h + k_i \bar{\mathbf{t}}), \\ h'_i(\mathbf{R}, \bar{\mathbf{t}}) &= \mathbf{e}_3^\top (\mathbf{R}\mathbf{y}_i^h + k_i \bar{\mathbf{t}}), \\ \mathbf{u}'_i(\mathbf{R}, \bar{\mathbf{t}}) &= \frac{\mathbf{W}(\mathbf{R}\mathbf{y}_i^h + k_i \bar{\mathbf{t}})}{\mathbf{e}_3^\top (\mathbf{R}\mathbf{y}_i^h + k_i \bar{\mathbf{t}})}. \end{aligned}$$

Let  $\Sigma = \sigma^2 \mathbf{I}_2$ , then given Assumption 3, the likelihood function is

$$\mathcal{L}(\mathbf{R}, \bar{\mathbf{t}}; \mathbf{z}) = \prod_{i=1}^m \frac{1}{2\pi\sigma^2} \exp\left(-\frac{1}{2} \|(\mathbf{z}_i - \mathbf{u}'_i(\mathbf{R}, \bar{\mathbf{t}}))\|_\Sigma^2\right),$$

which further yields the log-likelihood function

$$\ell(\mathbf{R}, \bar{\mathbf{t}}; \mathbf{z}) = m \ln \frac{1}{2\pi\sigma^2} - \sum_{i=1}^m \frac{1}{2} \|(\mathbf{z}_i - \mathbf{u}'_i(\mathbf{R}, \bar{\mathbf{t}}))\|_\Sigma^2. \quad (29)$$

Let  $\xi_{\mathbf{R}} = \text{vec}(\mathbf{R})$  and  $\xi = [\xi_{\mathbf{R}}^\top \bar{\mathbf{t}}^\top]^\top$ . The derivative of  $\ell(\mathbf{R}, \bar{\mathbf{t}}; \mathbf{z})$  is

$$\frac{\partial \ell}{\partial \xi^\top} = \sum_{i=1}^m (\mathbf{z}_i - \mathbf{u}'_i(\mathbf{R}, \bar{\mathbf{t}}))^\top \Sigma^{-1} \frac{\partial \mathbf{u}'_i}{\partial \xi^\top}.$$

To obtain  $\partial \mathbf{u}'_i / \partial \xi^\top$ , we need to calculate  $\partial \mathbf{u}'_i / \partial \xi_{\mathbf{R}}^\top$  and  $\partial \mathbf{u}'_i / \partial \bar{\mathbf{t}}^\top$ , respectively. The result is,

$$\begin{aligned} \frac{\partial \mathbf{u}'_i}{\partial \xi_{\mathbf{R}}^\top} &= \frac{h'_i \left( \mathbf{W} \mathbf{L}_i + \mathbf{W} \bar{\mathbf{t}} \frac{\partial k_i}{\partial \xi_{\mathbf{R}}^\top} \right) - \mathbf{g}'_i \left( \mathbf{e}_3^\top \mathbf{L}_i + \mathbf{e}_3^\top \bar{\mathbf{t}} \frac{\partial k_i}{\partial \xi_{\mathbf{R}}^\top} \right)}{h_i'^2}, \\ \frac{\partial \mathbf{u}'_i}{\partial \bar{\mathbf{t}}^\top} &= \frac{h'_i \left( \mathbf{W} k_i + \mathbf{W} \bar{\mathbf{t}} \frac{\partial k_i}{\partial \bar{\mathbf{t}}^\top} \right) - \mathbf{g}'_i \left( \mathbf{e}_3^\top k_i + \mathbf{e}_3^\top \bar{\mathbf{t}} \frac{\partial k_i}{\partial \bar{\mathbf{t}}^\top} \right)}{h_i'^2}, \end{aligned}$$

where  $\partial k_i / \partial \xi_{\mathbf{R}}^\top$  and  $\partial k_i / \partial \bar{\mathbf{t}}^\top$  are given in (25), and den and num represent the denominator and numerator of  $k_i$  in (22), respectively.

Then we have  $\partial \mathbf{u}'_i / \partial \xi^\top = [\partial \mathbf{u}'_i / \partial \xi_{\mathbf{R}}^\top \quad \partial \mathbf{u}'_i / \partial \bar{\mathbf{t}}^\top]^\top$ . Note that  $\mathbf{z}_i - \mathbf{u}'_i(\mathbf{R}^o, \bar{\mathbf{t}}^o) = \epsilon_i$ . Hence, the Fisher information matrix can be calculated as

$$\begin{aligned} \mathbf{F} &= \mathbb{E} \left[ \frac{\partial \ell}{\partial \xi} \frac{\partial \ell}{\partial \xi^\top} \right] \\ &= \mathbb{E} \left[ \left( \sum_{i=1}^m \frac{\partial \mathbf{u}'_i}{\partial \xi} \Sigma^{-1} \epsilon_i \right) \left( \sum_{i=1}^m \epsilon_i^\top \Sigma^{-1} \frac{\partial \mathbf{u}'_i}{\partial \xi^\top} \right) \right] \\ &= \sum_{i=1}^m \frac{\partial \mathbf{u}'_i}{\partial \xi} \Sigma^{-1} \frac{\partial \mathbf{u}'_i}{\partial \xi^\top}, \end{aligned}$$

where the third line is derived based on the independence among measurement noises  $\epsilon_i$ 's. Note that what we have now derived is unconstrained Fisher information. Since there are constraints on the rotation matrix  $\mathbf{R}$  and the normalized translation  $\bar{\mathbf{t}}$ , we need to calculate a constrained counterpart  $\mathbf{F}_c$ . We can use the following 7 equations to characterize the constraints

$$\mathbf{h}(\xi) = \begin{bmatrix} \xi_{1:3}^\top \xi_{1:3} - 1 \\ \xi_{4:6}^\top \xi_{1:3} \\ \xi_{7:9}^\top \xi_{1:3} \\ \xi_{4:6}^\top \xi_{4:6} - 1 \\ \xi_{7:9}^\top \xi_{4:6} \\ \xi_{7:9}^\top \xi_{7:9} - 1 \\ \xi_{10:12}^\top \xi_{10:12} - 1 \end{bmatrix} = \mathbf{0},$$

where the first 6 equations are associated with the rotation matrix [44] and the last one is for the normalized translation. Let

$$\mathbf{H}(\xi) = \frac{\partial \mathbf{h}(\xi)}{\partial \xi^\top} \in \mathbb{R}^{7 \times 12}.$$

The gradient matrix  $\mathbf{H}(\xi)$  have full row rank since the constraints are nonredundant, and hence there exists a matrix  $\mathbf{U} \in \mathbb{R}^{12 \times 5}$  whose columns form an orthonormal basis for the nullspace of  $\mathbf{H}(\xi)$ , that is,

$$\mathbf{H}(\xi) \mathbf{U} = \mathbf{0}$$

where  $\mathbf{U}^\top \mathbf{U} = \mathbf{I}$ . Finally, the constrained Fisher information is given as [45]

$$\mathbf{F}_c = \mathbf{U}(\mathbf{U}^\top \mathbf{F} \mathbf{U})^{-1} \mathbf{U}^\top,$$

and the theoretical lower bound is  $\text{CRB} = \text{tr}(\mathbf{F}_c)$ .

## REFERENCES

- [1] R. Hartley and A. Zisserman, *Multiple view geometry in computer vision*. Cambridge University Press, 2003.
- [2] J. Engel, V. Koltun, and D. Cremers, "Direct sparse odometry," *IEEE Transactions on Pattern Analysis and Machine Intelligence*, vol. 40, no. 3, pp. 611–625, 2017.
- [3] P.-E. Sarlin, P. Lindenberger, V. Larsson, and M. Pollefeys, "Pixel-perfect structure-from-motion with featuremetric refinement," *IEEE Transactions on Pattern Analysis and Machine Intelligence*, 2023, DOI: 10.1109/TPAMI.2023.3237269.
- [4] H. Zhan, C. S. Weerasekera, J.-W. Bian, and I. Reid, "Visual odometry revisited: What should be learnt?" in *Proceedings of IEEE International Conference on Robotics and Automation (ICRA)*, 2020, pp. 4203–4210.
- [5] R. I. Hartley, "In defense of the eight-point algorithm," *IEEE Transactions on Pattern Analysis and Machine Intelligence*, vol. 19, no. 6, pp. 580–593, 1997.
- [6] D. Nistér, "An efficient solution to the five-point relative pose problem," *IEEE Transactions on Pattern Analysis and Machine Intelligence*, vol. 26, no. 6, pp. 756–770, 2004.
- [7] B. Li, L. Heng, G. H. Lee, and M. Pollefeys, "A 4-point algorithm for relative pose estimation of a calibrated camera with a known relative rotation angle," in *Proceedings of IEEE/RSJ International Conference on Intelligent Robots and Systems (IROS)*, 2013, pp. 1595–1601.
- [8] A. Chatterjee and V. M. Govindu, "Robust relative rotation averaging," *IEEE Transactions on Pattern Analysis and Machine Intelligence*, vol. 40, no. 4, pp. 958–972, 2017.
- [9] D. Zou and P. Tan, "Coslam: Collaborative visual slam in dynamic environments," *IEEE Transactions on Pattern Analysis and Machine Intelligence*, vol. 35, no. 2, pp. 354–366, 2012.
- [10] Y.-Y. Jau, R. Zhu, H. Su, and M. Chandraker, "Deep keypoint-based camera pose estimation with geometric constraints," in *Proceedings of IEEE/RSJ International Conference on Intelligent Robots and Systems (IROS)*, 2020, pp. 4950–4957.
- [11] J. Zhao, "An efficient solution to non-minimal case essential matrix estimation," *IEEE Transactions on Pattern Analysis and Machine Intelligence*, vol. 44, no. 4, pp. 1777–1792, 2020.
- [12] G. Chesi, "Camera displacement via constrained minimization of the algebraic error," *IEEE Transactions on Pattern Analysis and Machine Intelligence*, vol. 31, no. 2, pp. 370–375, 2008.
- [13] U. Helmke, K. Hüper, P. Y. Lee, and J. Moore, "Essential matrix estimation using gauss-newton iterations on a manifold," *International Journal of Computer Vision*, vol. 74, pp. 117–136, 2007.
- [14] J. Briales, L. Kneip, and J. Gonzalez-Jimenez, "A certifiably globally optimal solution to the non-minimal relative pose problem," in *Proceedings of IEEE Conference on Computer Vision and Pattern Recognition (CVPR)*, 2018, pp. 145–154.
- [15] Y. Ding, D. Barath, J. Yang, H. Kong, and Z. Kukelova, "Globally optimal relative pose estimation with gravity prior," in *Proceedings of IEEE/CVF Conference on Computer Vision and Pattern Recognition (CVPR)*, 2021, pp. 394–403.
- [16] R. I. Hartley and F. Kahl, "Global optimization through rotation space search," *International Journal of Computer Vision*, vol. 82, no. 1, pp. 64–79, 2009.
- [17] N. Jiang, Z. Cui, and P. Tan, "A global linear method for camera pose registration," in *Proceedings of IEEE International Conference on Computer Vision (ICCV)*, 2013, pp. 481–488.
- [18] Y. Ma, J. Koščeká, and S. Sastry, "Optimization criteria and geometric algorithms for motion and structure estimation," *International Journal of Computer Vision*, vol. 44, pp. 219–249, 2001.
- [19] R. Tron and K. Daniilidis, "The space of essential matrices as a riemannian quotient manifold," *SIAM Journal on Imaging Sciences*, vol. 10, no. 3, pp. 1416–1445, 2017.
- [20] M. Garcia-Salguero, J. Briales, and J. Gonzalez-Jimenez, "A tighter relaxation for the relative pose problem between cameras," *Journal of Mathematical Imaging and Vision*, vol. 64, no. 5, pp. 493–505, 2022.
- [21] H. Li, R. Hartley, and J.-h. Kim, "A linear approach to motion estimation using generalized camera models," in *Proceedings of IEEE Conference on Computer Vision and Pattern Recognition (CVPR)*, 2008, pp. 1–8.
- [22] T. Schops, J. L. Schonberger, S. Galliani, T. Sattler, K. Schindler, M. Pollefeys, and A. Geiger, "A multi-view stereo benchmark with high-resolution images and multi-camera videos," in *Proceedings of IEEE Conference on Computer Vision and Pattern Recognition (CVPR)*, 2017, pp. 3260–3269.
- [23] M. J. Schervish, *Theory of statistics*. Springer Science & Business Media, 2012.
- [24] Z. Kukelova and T. Pajdla, "Two minimal problems for cameras with radial distortion," in *Proceedings of IEEE International Conference on Computer Vision (ICCV)*, 2007, pp. 1–8.
- [25] Z. Kukelova, M. Bujnak, and T. Pajdla, "Polynomial eigenvalue solutions to the 5-pt and 6-pt relative pose problems," in *Proceedings of British Machine Vision Conference (BMVC)*, 2008, pp. 56.1–56.10.
- [26] H. Stewenius, C. Engels, and D. Nistér, "Recent developments on direct relative orientation," *ISPRS Journal of Photogrammetry and Remote Sensing*, vol. 60, no. 4, pp. 284–294, 2006.
- [27] L. Kneip, R. Siegwart, and M. Pollefeys, "Finding the exact rotation between two images independently of the translation," in *Proceedings of European Conference on Computer Vision (ECCV)*, 2012, pp. 696–709.
- [28] H. C. Longuet-Higgins, "A computer algorithm for reconstructing a scene from two projections," *Nature*, vol. 293, no. 5828, pp. 133–135, 1981.
- [29] D. Barath and J. Matas, "Graph-cut ransac: Local optimization on spatially coherent structures," *IEEE Transactions on Pattern Analysis and Machine Intelligence*, vol. 44, no. 9, pp. 4961–4974, 2021.
- [30] R. Subbarao, Y. Genc, and P. Meer, "Robust unambiguous parametrization of the essential manifold," in *Proceedings of IEEE Conference on Computer Vision and Pattern Recognition (CVPR)*, 2008, pp. 1–8.
- [31] L. Kneip and S. Lynen, "Direct optimization of frame-to-frame rotation," in *Proceedings of IEEE International Conference on Computer Vision (ICCV)*, 2013, pp. 2352–2359.
- [32] S. P. Boyd and L. Vandenberghe, *Convex optimization*. Cambridge University Press, 2004.
- [33] M. Garcia-Salguero, J. Briales, and J. Gonzalez-Jimenez, "Certifiable relative pose estimation," *Image and Vision Computing*, vol. 109, 2021, Art. no. 104142.
- [34] V. Lepetit, F. Moreno-Noguer, and P. Fua, "Epnp: An accurate o(n) solution to the pnp problem," *International Journal of Computer Vision*, vol. 81, no. 2, pp. 155–166, 2009.
- [35] J. A. Hesch and S. I. Roumeliotis, "A direct least-squares (dls) method for pnp," in *Proceedings of IEEE International Conference on Computer Vision (ICCV)*, 2011, pp. 383–390.
- [36] S. Urban, J. Leitloff, and S. Hinz, "Mlpnp-a real-time maximum likelihood solution to the perspective-n-point problem," *arXiv:1607.08112*, 2016.
- [37] E. L. Lehmann and G. Casella, *Theory of point estimation*. Springer Science & Business Media, 2006.
- [38] Q. Cai, Y. Wu, L. Zhang, and P. Zhang, "Equivalent constraints for two-view geometry: Pose solution/pure rotation identification and 3d reconstruction," *International Journal of Computer Vision*, vol. 127, pp. 163–180, 2019.
- [39] C. Campos, R. Elvira, J. J. G. Rodríguez, J. M. Montiel, and J. D. Tardós, "Orb-slam3: An accurate open-source library for visual, visual-inertial, and multimap slam," *IEEE Transactions on Robotics*, vol. 37, no. 6, pp. 1874–1890, 2021.
- [40] C. Toft, W. Maddern, A. Torii, L. Hammarstrand, E. Stenborg, D. Safari, M. Okutomi, M. Pollefeys, J. Sivic, T. Pajdla, F. Kahl, and T. Sattler, "Long-term visual localization revisited," *IEEE Transactions on Pattern Analysis and Machine Intelligence*, vol. 44, no. 4, pp. 2074–2088, 2020.
- [41] A. Tonioni, M. Poggi, S. Mattoccia, and L. Di Stefano, "Unsuper-vised domain adaptation for depth prediction from images," *IEEE Transactions on Pattern Analysis and Machine Intelligence*, vol. 42, no. 10, pp. 2396–2409, 2019.
- [42] G. Zeng, B. Mu, L. Shi, J. Chen, and J. Wu, "Consistent and asymptotically efficient localization from range-difference measurements," *arXiv:2302.03311*, 2023.
- [43] G. Zeng, B. Mu, J. Chen, Z. Shi, and J. Wu, "Global and asymptotically efficient localization from range measurements," *IEEE Transactions on Signal Processing*, vol. 70, pp. 5041–5057, 2022.
- [44] K. M. Lynch and F. C. Park, *Modern robotics*. Cambridge University Press, 2017.
- [45] P. Stoica and B. C. Ng, "On the cramer-rao bound under parametric constraints," *IEEE Signal Processing Letters*, vol. 5, no. 7, pp. 177–179, 1998.